NAVAL POSTGRADUATE SCHOOL
Monterey, California

THESIS

MICROMECHANICAL STUDY OF INTERFACE STRESS IN A FIBER-REINFORCED COMPOSITE UNDER TRANSVERSE LOADING USING BOUNDARY ELEMENT METHOD

by

Hakan Eren

March 2000

Thesis Advisor: Young W. Kwon

DTIC QUALITY INSPECTED 4

REPORT DOCUMENTATION PAGE

Form Approved OMB No. 0704-0188

Public reporting burden for this collection of information is estimated to average 1 hour per response, including the time for reviewing instruction, searching existing data sources, gathering and maintaining the data needed, and completing and reviewing the collection of information. Send comments regarding this burden estimate or any other aspect of this collection of information, including suggestions for reducing this burden, to Washington Headquarters Services, Directorate for Information Operations and Reports, 1215 Jefferson Davis Highway, Suite 1204, Arlington, VA 22202-4302, and to the Office of Management and Budget, Paperwork Reduction Project (0704-0188) Washington DC 20503.

1. AGENCY USE ONLY *(Leave blank)*	2. REPORT DATE March 2000	3. REPORT TYPE AND DATES COVERED Master's Thesis

4. TITLE AND SUBTITLE: Micro mechanical Study of Interface Stress in a Fiber-Reinforced Composite Under Transverse Loading Using Boundary Element Method	5. FUNDING NUMBERS
6. AUTHOR(S) Eren, Hakan	

7. PERFORMING ORGANIZATION NAME(S) AND ADDRESS(ES) Naval Postgraduate School Monterey CA 93943-5000	8. PERFORMING ORGANIZATION REPORT NUMBER

9. SPONSORING/MONITORING AGENCY NAME(S) AND ADDRESS(ES)	10. SPONSORING/MONITORING AGENCY REPORT NUMBER

11. SUPPLEMENTARY NOTES
The views expressed here are those of the authors and do not reflect the official policy or position of the Department of Defense or the U.S. Government.

12a. DISTRIBUTION/AVAILABILITY STATEMENT Approved for public release; distribution is unlimited.·	12b. DISTRIBUTION CODE

13. ABSTRACT *(maximum 200 words* Composite materials are involving in engineering applications at a growing speed, due to their stiffer, stronger and lighter properties. This growth requires fast and powerful numerical methods like Boundary Element Method (BEM), and Finite Element Method (FEM). BEM has become popular especially in the last decade due to its advantage of requiring less computation time for the same accuracy. The objective of this study is, by using Boundary Element Method, to examine different shapes of reinforcement elements under unit traction and unit displacement boundary conditions in transversal direction and perfect interfacial bonding. The stress variations along the interface of the matrix and reinforcing material, effective elastic modulus of composites were studied due to different shapes and different volume fractions of reinforcement elements. These calculations were made for both the internal Representative Volume Element (RVE), and boundary RVE, which are the internal and boundary cells of composite material respectively. Finally, using an appropriate failure criterion, the failures of different shapes were examined and also the effective elastic modulus variations of the shapes during the progress of the failure for both internal and boundary RVE were studied.

14. SUBJECT TERMS Micro mechanics, Interface, Boundary element method, Debonding		15. NUMBER OF PAGES 90
		16. PRICE CODE

17. SECURITY CLASSIFICATION OF REPORT Unclassified	18. SECURITY CLASSIFICATION OF THIS PAGE Unclassified	19. SECURITY CLASSIFICATION OF ABSTRACT Unclassified	20. LIMITATION OF ABSTRACT UL

NSN 7540-01-280-5500

Standard Form 298 (Rev. 2-89)
Prescribed by ANSI Std. 239-18 298-102

i

MICROMECHANICAL STUDY OF INTERFACE STRESS IN A FIBER-REINFORCED COMPOSITE UNDER TRANSVERSE LOADING USING BOUNDARY ELEMENT METHOD

Hakan Eren
Lieutenant Junior Grade, Turkish Navy
B.S. Naval Architecture, Turkish Naval Academy1994

Submitted in partial fulfillment of the
requirements for the degree of

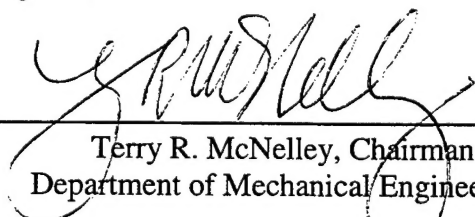## MASTER OF SCIENCE IN MECHANICAL ENGINEERING

from the

NAVAL POSTGRADUATE SCHOOL
March 2000

Author: _____
Hakan Eren

Approved by: _____
Young W. Kwon, Thesis Advisor

_____
Terry R. McNelley, Chairman
Department of Mechanical Engineering

iii

ABSTRACT

Composite materials are involving in engineering applications at a growing speed, due to their stiffer, stronger and lighter properties. This growth requires fast and powerful numerical methods like Boundary Element Method (BEM), and Finite Element Method (FEM). BEM has become popular especially in the last decade due to its advantage of requiring less computation time for the same accuracy. The objective of this study is, by using Boundary Element Method, to examine different shapes of reinforcement elements under unit displacement boundary conditions in transversal direction and at perfect interfacial bonding. The stress variations along the interface of the matrix and reinforcing material, effective elastic modulus of composites were studied due to different shapes and different volume fractions of reinforcement elements. These calculations were made for both the internal Representative Volume Element (RVE), and boundary RVE, which are the internal and boundary cells of composite material respectively. Finally, using an appropriate failure criterion, the failures of different shapes were examined and also the effective elastic modulus variations of the shapes during the progress of the failure for both internal and boundary RVE were studied.

TABLE OF CONTENTS

I. INTRODUCTION

Composite materials have attracted the attention of researchers for the past decades because of their beneficial properties that can not be met by conventional metals, like high specific strength, high specific stiffness, etc. Composite material production is an important process. This process is a combination of different phases that have been brought together at certain proportions and at an appropriate processing in order to make a different material that has better properties than the constituents individually. Many composite materials composed of two phases, one of which is called the matrix element and the other is called the reinforcement or the fiber element. These phases come together at the interface. The matrix material surrounds the reinforcement material, binds the reinforcement elements, absorbs a small amount of the load, protects the individual fibers from surface damage, and it behaves as a barrier for the crack propagation. Because of these reasons, the matrix material is softer than the reinforcement material with some required ductility.

The properties of the composite materials also depend on the volume fraction of the individual materials, the orientation of the reinforcement material, the bonding at the interface etc. Interface failure affects the strength and stiffness of composite materials significantly. Furthermore, interface failure is susceptible to transverse loading. Therefore, this study investigated the interface stress distribution to better understand possible interface failure initiation and growth and its effect on the composite materials.

THIS PAGE INTENTIONALLY LEFT BLANK

II. BACKGROUND

A. LITERATURE SURVEY

Boundary element method (BEM) has been used more often for the last decade due to its well-known advantage of reduction of dimension by one. In boundary element method, instead of whole body, only the boundary needs to be discretized. With less computation time, same level of accuracy can be achieved.

Achenbach and Zhu [Ref. 1], using BEM, worked on composites that have only circular shape fiber, and subjected to a uniform stress in transversal direction. In this study, an additional very thin interfacial zone was considered, and the calculations were done for a certain fiber volume fraction, 50%, certain elastic modulus values, 0.7×10^3 MPa and 5.5×10^3 MPa for the matrix and fiber materials respectively, and Poisson's ratio for the matrix and fiber materials, 0.33 and 0.25 respectively. The effects of interfacial zone for the elastic module of both fiber and matrix materials at different stiffness values without any crack and with some crack length were studied. Without any debonding, the stress values along the boundary and symmetry line perpendicular to the applied stress direction were calculated. It was found that the initiation of the crack would occur along the interface close to the applied stress. They have also included the effective stress strain curve of the composite, with and without any interface crack to the study.

Shen, Finot, Needleman and Suresh [Ref. 2], worked on the overall elastic properties of two-phased discontinuously reinforced composites as a function of shape and spatial distribution of the reinforcement using Finite Element Analysis. Like in our study, the materials were taken to be isotropic and the interface was perfectly bonded. It was found that circular shape reinforcement element gave the highest effective elastic

3

modulus and the distribution of the reinforcement for the same volume fraction gave different effective elastic modulus values, and it was observed that double reinforcement case with equal volume fraction each gave the lowest effective elastic modulus. The increase in elastic modulus values increased with increasing concentration of the reinforcement. They also worked on the effects of particle cracking on effective elastic modulus of composites, and did not work on debonding of the interface.

Pan, Adams and Rizzo [Ref. 3], conducted a study based on two-dimensional micro mechanical behavior of fiber-reinforced composites. One of the objectives of the study was to find the effective elastic modulus variation of the composite material due to different volume fractions of reinforcement material, and also due to different elastic modulus ratios of reinforcement material to the matrix material. The interface bonding was assumed to be both perfectly and imperfectly bonded. The composite material that has only circular shape reinforcement element with a unit traction boundary condition was studied using BEM. For the volume fraction, two different volume fractions were used; 55 and 70% for the calculations of normalized effective elastic modulus at different shear modulus values. for the imperfectly bonded interface case, five different stiffness values for the interface were used and the stress strain curves for the composites and the stress values along the edge were calculated. It has been observed that the results, for perfectly bonded model, coincided satisfactorily with physical experiments and FEM.

Another study about micro and macro analysis of composites were made in a five year research conducted by NASA [Ref. 4] using Best-Cms engineering system based on BEM program Best3d. In Chapter VII of the research, effective elastic modulus of the composite were studied using specific elastic modulus and Poisson's ratios for the

4

materials. in the study, circular shape reinforcement was used for single and multiple cases which were subjected to tension and shear in the direction parallel and perpendicular to the fiber. The results were plotted for effective elastic modulus vs. fiber volume fraction values between 0 and 30%. Also, in the same chapter, the effect of fiber Poisson's ratio in the composite material was studied.

B.   OBJECTIVES

The objective of this study was, by using boundary element method, to find out fiber/matrix interface stress distribution for a perfectly bonded interface, due to its importance for interfacial debonding. Micro mechanical models for four different shapes of reinforcements; different reinforcement volume fractions, and different shear modulus ratios of fiber to matrix materials were modeled. The study was made for both internal and boundary RVEs of the composite material, because the inner and the boundary cells of the composite material respond differently and give different stress distributions from each other. This study also included the effect of interaction of different size and/or orientation of reinforcements along the interface stress. Furthermore, the effective elastic modules values were calculated for the cases without debonding and at different debonding ratios.   Other than single reinforcement case for a cell of the composite, double reinforcement case was also studied at two different cases, and the same analysis was conducted for this case also.

III.   BOUNDARY ELEMENT TECHNIQUES

A.   FORMULATION

The equations of equilibrium in 2-D solids is:

$$\sigma_{ji,j} + b_i = 0 \qquad\qquad i, j = 1, 2 \tag{3.1}$$

where σ_{ij} is the stress tensor and b_i is a body force. Boundary conditions associated with the differential equations are:

$$t_i = \sigma_{ji} n_j = \overline{t_i} \quad \text{on } \Gamma_1 \quad i, j = 1, 2 \tag{3.2}$$

$$u_i = \overline{u_i} \qquad\qquad \text{on } \Gamma_2 \qquad \text{or } i, j = 1, 2 \tag{3.3}$$

where $\Gamma_1 \cap \Gamma_2 = \emptyset$ and $\Gamma_1 \cup \Gamma_2 = \Gamma$. Here Γ represents the total boundary of the solid.

Applying the weighted residual method to Eq. (3.1) yields:

$$\int_{\Omega} (\sigma_{ji,j} + b_i) u_i^* d\Omega = 0 \tag{3.4}$$

in which u_i^* is the test function. Applying integration by parts to the first product term in Eq. (3.4) results in:

$$\int_{\Omega} b_i u_i^* d\Omega - \int_{\Omega} \sigma_{ji} u_{i,j}^* d\Omega + \int_{\Gamma} \sigma_{ji} n_j u_i^* d\Gamma = 0 \tag{3.5}$$

Here n_j is the direction cosine at the boundary with outward direction positive.

Knowing that:

$$\sigma_{ji} u_{i,j}^* = \frac{1}{2}(\sigma_{ji} u_{i,j}^* + \sigma_{ij} u_{j,i}^*) = \sigma_{ji} \frac{1}{2}(u_{i,j}^* + u_{j,i}^*) = \sigma_{ji} \varepsilon_{i,j}^* \tag{3.6}$$

and strain tensor is symmetric, Eq. (3.5) becomes:

$$\int_{\Omega} b_i u_i^* d\Omega - \int_{\Omega} \sigma_{ji} \varepsilon_{ji}^* d\Omega + \int_{\Gamma} \sigma_{ji} n_j u_i^* d\Gamma = 0 \tag{3.7}$$

7

Use of $\sigma_{ji}\varepsilon_{ji}^* = \sigma_{ji}^*\varepsilon_{ji} = \sigma_{ji}^*u_{i,j}$ and integration by parts to Eq. (3.7) yields:

$$\int_\Omega b_i u_i^* d\Omega + \int_\Omega b_i u_i \sigma_{ji,j}^* d\Omega - \int_\Gamma u_i n_j \sigma_{ji}^* d\Gamma + \int_\Gamma \sigma_{ji} n_j u_i^* d\Gamma = 0 \qquad (3.8)$$

or

$$\int_\Omega b_i u_i^* d\Omega + \int_\Omega u_i \sigma_{ji,j}^* d\Omega - \int_\Gamma u_i t_i^* d\Gamma + \int_\Gamma t_i u_i^* d\Gamma = 0 \qquad (3.9)$$

where traction $t_i = \sigma_{ji} n_j$.

Define $\sigma_{ji,j}^*$ such that:

$$\sigma_{ji,j}^* = -\delta_n(\underline{x} - \underline{\zeta}) \qquad (3.10)$$

where $\delta_n(\underline{x} - \underline{\zeta})$ is the Dirac delta function and represents a unit load at $\underline{\zeta}$ in the n

direction. Then Eq. (3.9) becomes:

$$\int_\Omega b_i u_{ni}^* d\Omega - u_n(\zeta) - \int_\Gamma u_i t_{ni}^* d\Gamma + \int_\Gamma t_i u_{ni}^* d\Gamma = 0 \qquad (3.11)$$

or

$$u_n^m (= u_n(\underline{\zeta}) + \int_\Gamma u_i t_{ni}^* d\Gamma = \int_\Gamma t_i u_{ni}^* d\Gamma + \int_\Omega b_i u_{ni}^* d\Omega \qquad (3.12)$$

where t_{ni}^* and u_{ni}^* are the tractions and displacements in the i direction due to a unit force

acting in the n direction. This is the boundary integral equation to be discretized along

the boundary.

The solution satisfying Eq. (3.10) with the plane strain condition is:

$$u_{ni}^* = \frac{1}{8\pi G(1-v)}\left[(3-4v)\ln(\frac{1}{r})\delta_{ni} + \frac{\partial r}{\partial x_n}\frac{\partial r}{\partial x_i}\right] \qquad (3.13)$$

and

$$t_{ni}^* = -\frac{1}{4\pi(1-v)r}\left[\frac{\partial r}{\partial n}\left\{(1-2v)\delta_{ni}+\frac{\partial r}{\partial x_n}\frac{\partial r}{\partial x_i}\right\}-(1-2v)\left(\frac{\partial r}{\partial x_n}n_i-\frac{\partial r}{\partial x_i}n_n\right)\right] \quad (3.14)$$

Discretizing the boundary with a number of elements with no body force results

in:

$$C^m u^m + \int_\Gamma t^* u d\Gamma = \int_\Gamma u^* t d\Gamma \quad (3.15)$$

or

$$C^m u^m + \sum_{j=1}^{NE} H_{mj} u_j = \sum_{j=1}^{NE} G_{mj} t_j \quad (3.16)$$

Eq. (3.16) can be written as:

$$[H]\{U\} = [G]\{T\} \quad (3.17)$$

The details can be found in Reference 5.

B. MODELING

In composite materials, the cross-sectional shapes of reinforcement are not uniform. However, in real applications, it is neither possible nor practical to get their exact shapes. Thus, modeling the reinforcement material in a certain shape makes the calculations much easier. In this study, four different reinforcement shapes were studied, which are; circular, diamond, octagonal and square shapes (See Figure 3.1). For the circular shape of reinforcement, volume fraction was varied from 20 to 70 percent for different volume fraction and shear modulus ratio study. For comparison of different shapes and other cases, 40 percent volume fraction was used.

For the modeling of single reinforcement case, only one cell of the composite material, that has one reinforcement material at the center, was selected. Since it is symmetric about its vertical and horizontal axis, only one quarter of it was taken for simplicity (See Figure 3.2). The outer dimensions of the model were taken as unity, and the dimensions of the reinforcement elements were calculated due to their volume fractions.

The node numbering was done for each material separately, starting from reinforcement material in counterclockwise direction and, followed by the matrix material. After the node numbering, the x and y coordinate values for each node were assigned. The elements, connecting the nodes were numbered in the same way. Then, the numbered elements were connected by the nodes on each side of the corresponding elements. The elements along EF in the Figure 3.2 are the interface elements, where the matrix and the reinforcement materials meet. The rest of the elements are the boundary elements.

The calculations were done for both internal and boundary Representative Volume Elements (RVE). According to the BEM program, code 0 means displacement and code 1 means traction. The boundary conditions were applied only to the boundary elements not to the interface elements. The applied boundary conditions are as follows (See Figure 3.2):

$t_x = 0, u_y = 0$ along AE and EB

$t_x = 0, t_y = 0$ along BC (BG and GC in Figure 3.3)

$t_x = 0, u_y = 1$ along CD (CH and HD in Figure 3.3)

$u_x = 0, t_y = 0$ along AF and FD

Along AE and EB of the composite material, due to symmetry there is no displacement in y direction. BC is the traction free surface for boundary RVE. For internal RVE, the elements along BC were moved same amount to the left along x-axis to maintain the symmetry with the next cell. CD is the boundary where unit displacement was applied. Along AF and FD, there is no displacement in x direction due to symmetry.

For the modeling of double reinforcement, only circular shape reinforcement was modeled for two cases. For the first case, each of the reinforcement had 20 percent volume fraction, and in the second case, one had 30 percent, the other had 10 percent volume fraction. Like in single reinforcement case, one quarter of the cell was taken because of symmetry (See Figure 3.3). The outer dimensions of the model, node numbering, connectivity, element numbering, boundary conditions were taken the same like in single reinforcement case. The dimensions of the reinforcements were calculated due to their volume fractions. In this case, there were two interfaces, EF and GH in

11

Figure 3.3. The calculations were made only for internal RVE and the stress values along the interfaces were calculated separately.

The Poisson's ratios of the reinforcement element and the matrix element were taken as 0.3 and 0.49 respectively for the study of stress and failure analysis. But, to compare the results of this study with some other studies, 0.22 for the reinforcements and 0.35 and 0.45 for the matrix material were used.

The interface elements, which are the elements of whose stress values are to be calculated, were entered to the main program separately.

The boundary element numbers, the total element numbers, the interface element numbers, the number of different zones, the last node of each zone, the coordinates of the nodes, the element connectivity, and the interface element numbering are calculated using Matlab programming. All the required data were gathered together in the output file of the Matlab program. This output file was used as an input file for the BEM calculating program. The results were discussed in the following chapters.
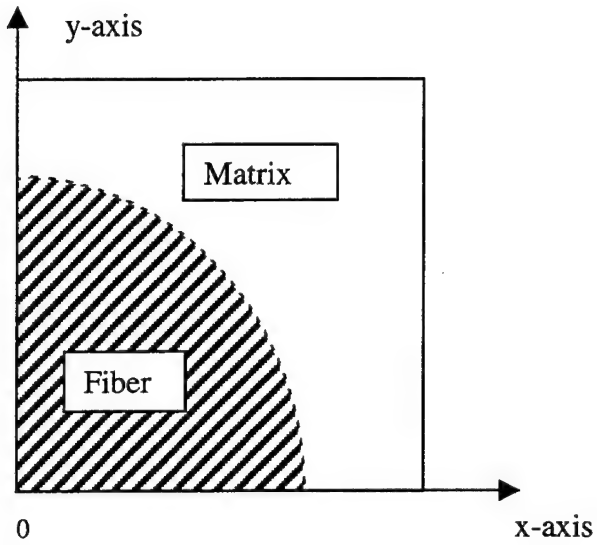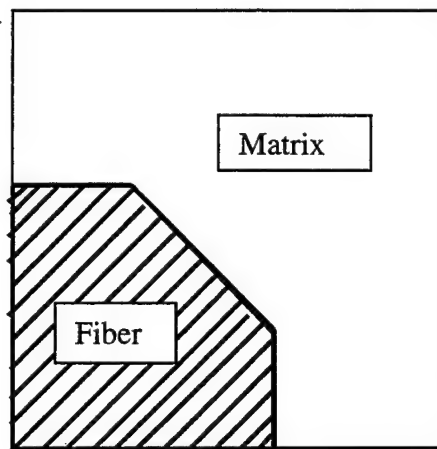
a. Circular shape
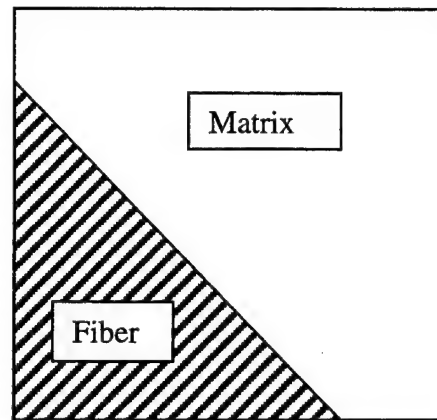
b. Diamond shape
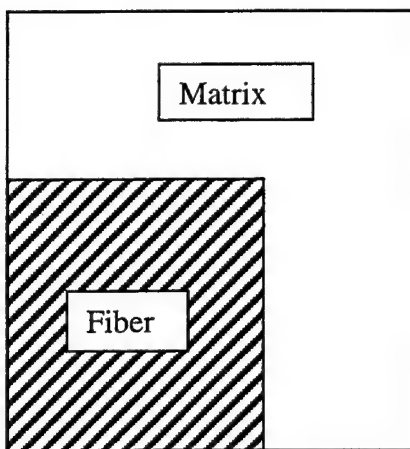
c. Square shape

d. Octagonal shape

Figure 3.1: Four Different Shapes of Reinforcement Materials.
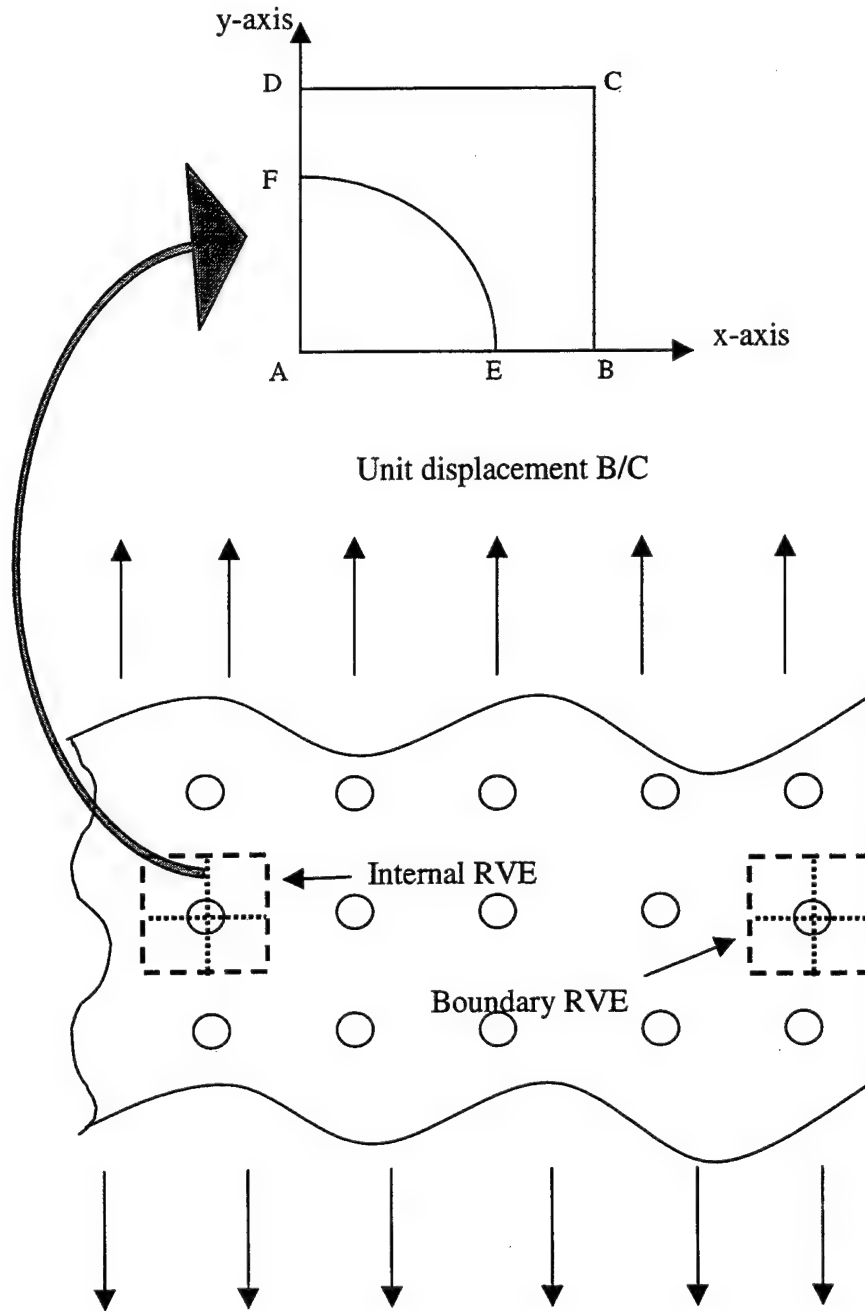
(SINGLE REINFORCEMENT CASE)

Figure 3.2: Modeling Demonstration of Circular Shape for Single Reinforcement Case.
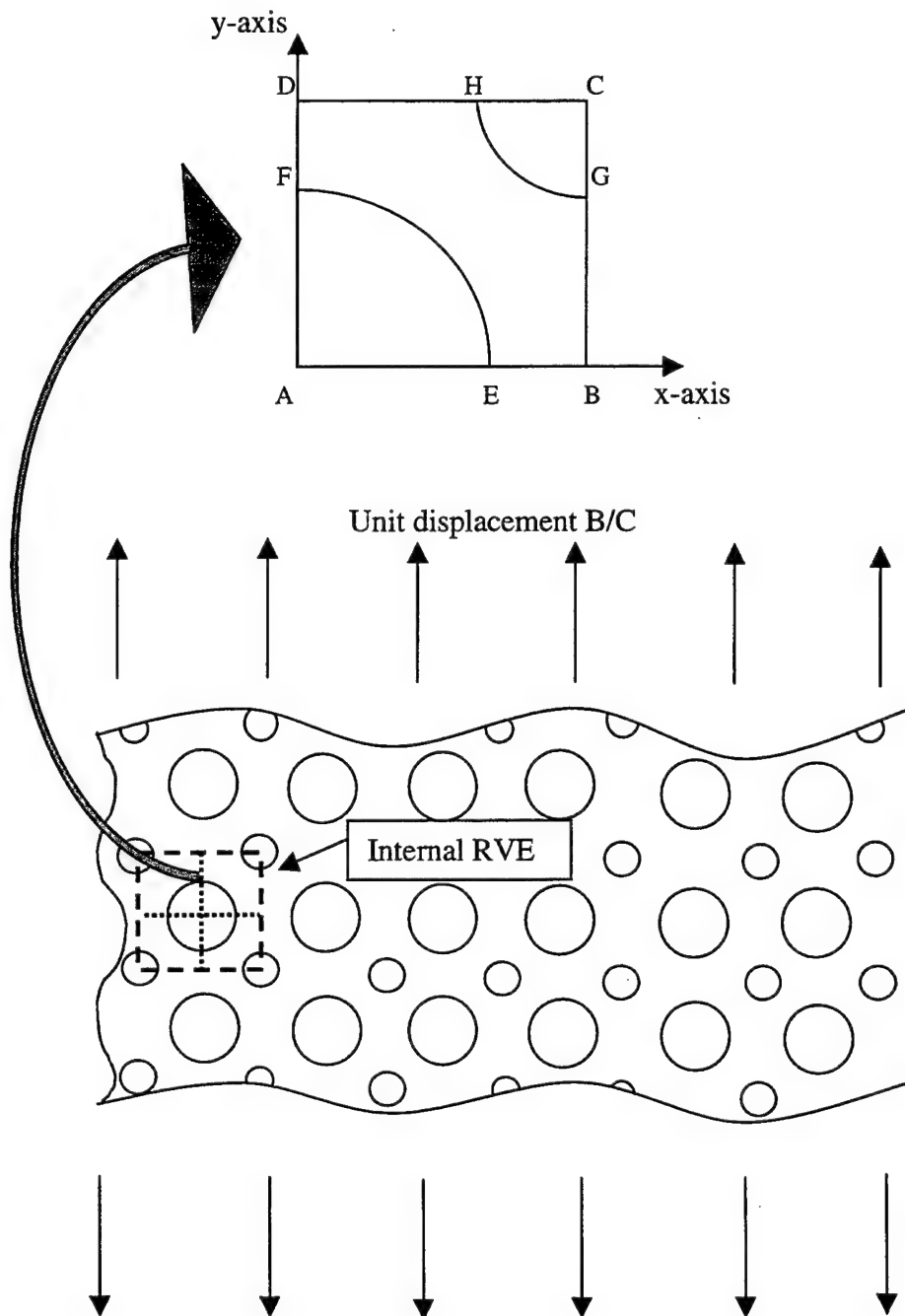
(DOUBLE REINFORCEMENT CASE)

Figure 3.3: Modeling Demonstration of Double Reinforcement Case for Circular Shape Composite Material.

THIS PAGE INTENTIONALLY LEFT BLANK

IV.   NUMERICAL SOLUTION VERIFICATION

A.   SOLUTION VERIFICATION

First of all, the formulation and computer program was checked by comparing the numerical result to a known analytical solution [Ref. 6]. The selected problem was an infinite plate with a circular reinforcement (See Figure 4.1). The plate had a circular hole at the center and was subjected to a uniaxial tensile load. A circular plate of the same size as the hole in the infinite plate was inserted into the hole. The case was considered to have perfect bonding (welding) at their interface.

The analytical solution is given below [Ref. 6]:

$$\sigma_{rr} = \frac{P}{2}\left[\beta_0 + \delta_0 Cos 2\theta\right] \qquad \text{(Normal stress)} \qquad (4.1)$$

$$\sigma_{\theta\theta} = \frac{P}{2}\left[\beta_0 + \left(\frac{6\gamma_0}{R^2}r^2 - \delta_0\right)Cos 2\theta\right] \qquad \text{(Hoop stress)} \qquad (4.2)$$

$$\sigma_{r\theta} = \frac{P}{2}\left[\frac{3\gamma_0}{R^2}r^2 - \delta_0\right]Sin 2\theta \qquad \text{(Shear stress)} \qquad (4.3)$$

The variable R represents the radius of the hole inside the infinite plate, and the variable r represents the radius of the plate that was welded into the hole. The variables that have 0 subscript represent the variables of the reinforcement element.

$$\chi = \left(\frac{\lambda + 3\mu}{\lambda + \mu}\right), \quad \mu_0 = \frac{E_0}{2(1+v_0)}, \quad \beta_0 = \frac{\mu_0(\chi+1)}{2\mu_0 + \mu(\chi_0 - 1)}, \quad \gamma_0 = 0$$

$$\delta_0 = \frac{\mu_0(\chi+1)}{\mu + \mu_0\chi}, \quad \mu = \frac{E}{2(1+v)}, \quad \lambda = \frac{Ev}{(1+v)(1-2v)} \qquad (4.4)$$

17

Furthermore, substitution of Equation (4.4) into Equations (4.1) and (4.3) yields the following normal and shear stresses at the interface:

$$\sigma_{rr} = \frac{P}{2}\left[\frac{\mu_0(\chi+1)}{2\mu_0+\mu(\chi_0-1)}+\frac{\mu_0(\chi+1)}{\mu+\mu_0\chi}Cos2\theta\right] \quad \text{(Normal stress)} \qquad (4.5)$$

$$\sigma_{\theta\theta} = \frac{P}{2}\left[\frac{\mu_0(\chi+1)}{2\mu_0+\mu(\chi_0-1)}+\frac{\mu_0(\chi+1)}{\mu+\mu_0\chi}Cos2\theta\right] \quad \text{(Tangential stress)} \qquad (4.6)$$

The same problem was solved using the boundary element method. The infinite plate was modeled as a large square plate whose dimension was much greater than the hole size. The hole size was 1/10 of the plate dimension. Only one quarter of the geometry was solved because of two symmetric axes as shown in Figure 4.1. Ten constant elements were used along each interface, respectively, and 160 elements were used along the rest of the boundary. The boundary ABC in Figure 4.1 has no vertical displacement and no tangential traction while boundary AFE has no horizontal displacement and no tangential traction because of symmetry. Furthermore, boundary DE has a unit uniform normal traction with zero tangential traction. Finally, boundary CD is free of traction in both normal and tangential directions. Along the interface boundary BF, stress and displacement continuity conditions were applied. In case of perfect welding, those continuities were maintained in both normal and tangential directions while the no-friction case, only the normal continuity condition was enforced with zero tangential traction.

The numerical solutions were compared to the analytical solutions in Figure 4.2. Both normal and tangential stresses at the interface were plotted in the figure as a function of the angle measured from the x-axis (See Figure 4.1). The angle varied from 0 to 90 degrees. The numerical solutions agreed well with the analytical solution. Especially, the normal stresses had a better agreement. The interface normal stress is in maximum tension along y-axis and in maximum compression along x-axis because of Poisson's effect. Poisson's ratio of the matrix element is greater than the Poisson's ratio of the reinforcement element, thus, contraction in the matrix element is greater than the reinforced material. This causes compression at the interface at lower angles. The tangential (shear) stress is the maximum in magnitude at the interface location of 45 degrees. In the same Figure, (Figure 4.2) at 45 degrees, the normal stress has 0.5 value which is the average of the maximum and the minimum normal stresses (principal stresses). In the tangential stress plot, there is a slight difference between analytical and numerical solutions. At 0 and 90 degrees at the interface, the tangential stresses have to be zero because of the symmetry, and the analytical solution agrees with this but there is a slight difference in the boundary element solution. This is because numerical methods do not give exact solution, but approximate solution. However, they have very close solutions. This comparison showed that the boundary element method gives pretty good and reliable results for this study.

B.   DIFFERENT NUMBERS OF ELEMENTS

In the analysis of boundary element method, different numbers of elements were tried at the interface, where all the attentions were focused. For the circular shape reinforcement element having 40 percent volume fraction in the cell, four different numbers of elements were used at the interface; 10, 40, 60, 80. As the boundary condition, unit traction boundary condition was used. Normal and tangential stresses were calculated at the interface, and the results were plotted in Figs. 4.3 and 4.4. In the comparison of these different numbers of elements, all cases give almost identical results, except 10 elements. 10 elements give very slightly different results from the others. As a result of this comparison, 40 elements, having the same result with the a less computation time, were selected along the interface of different shapes and different volume calculations.
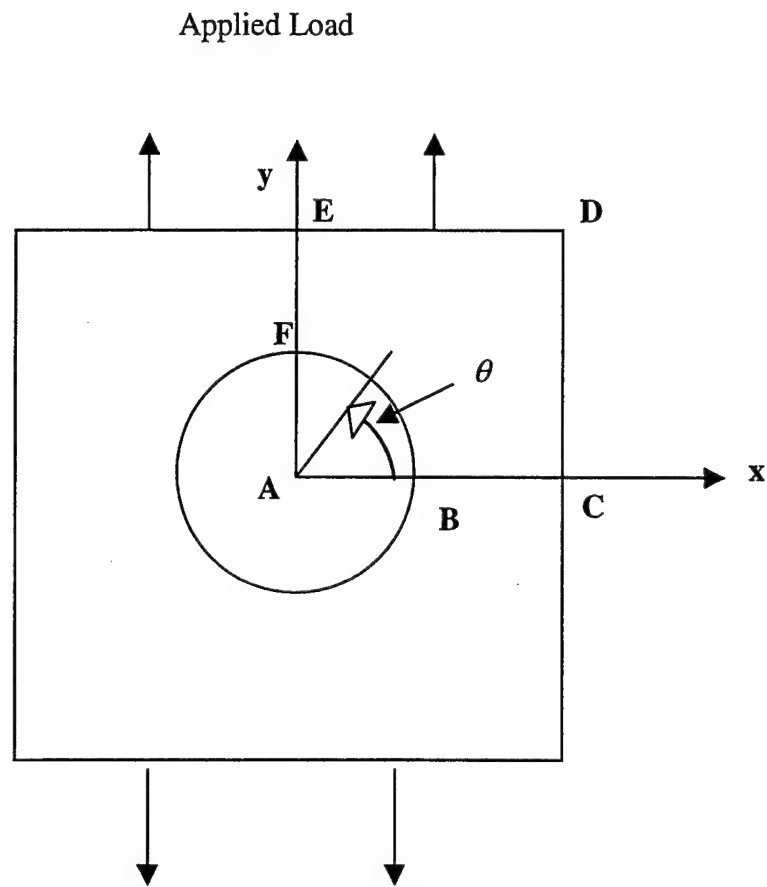
Figure 4.1: Unit Cell of a Composite Material that has a Circular Shape
Reinforcement Element.
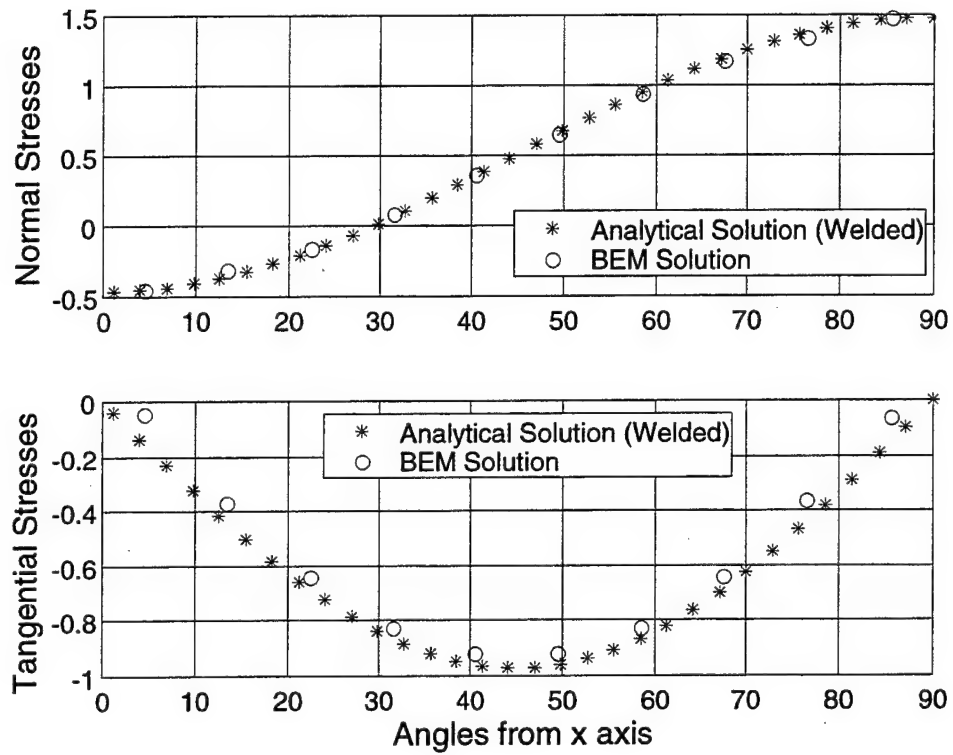
Figure 4.2: Analytical vs. BEM Calculation Comparison for Normal and tangential stresses.
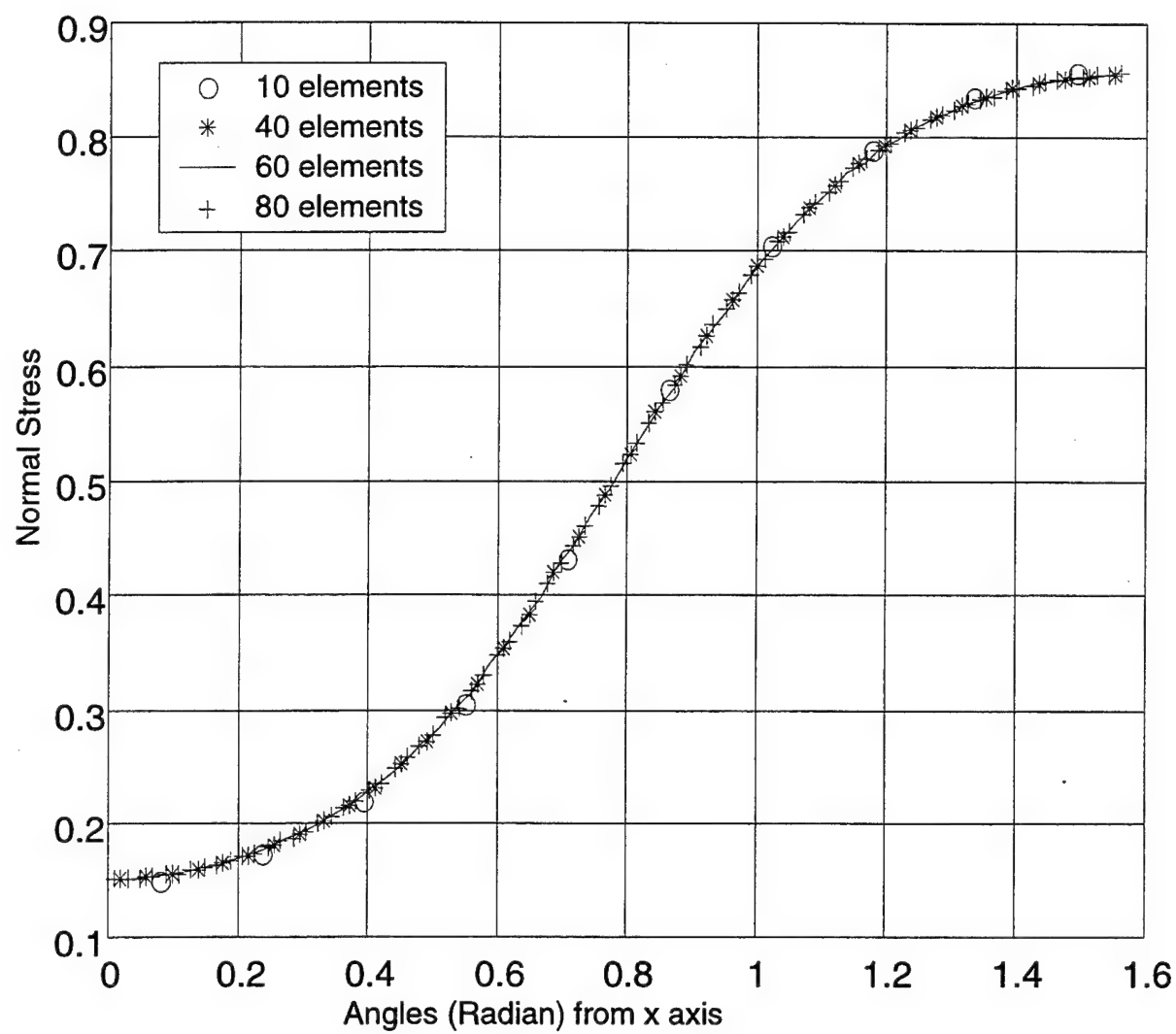
Figure 4.3: Normal Stresses along the Interface for Different Numbers of Interface Elements.
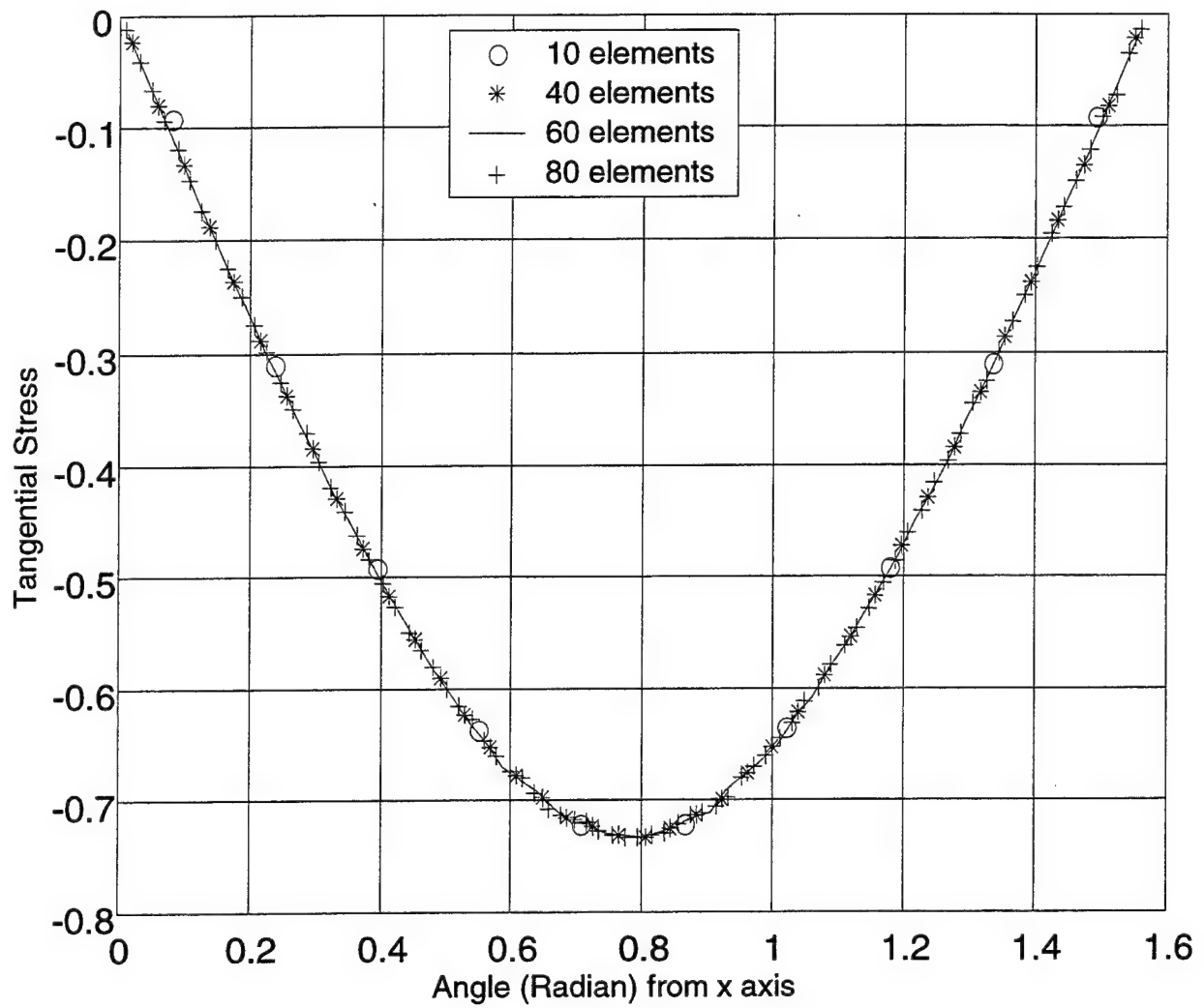
Figure 4.4: Tangential Stresses along the Interface for Different Numbers of Elements.

V.   RESULTS WITHOUT DEBONDING

A.   DIFFERENT SHAPE OF REINFORCEMENT ELEMENTS

Four different shapes of reinforcement as shown in Figure 3.1 were analyzed and compared in this section.   Each reinforcement had the same volume fraction as 40 percent, and shear modulus ratio (reinforcement modulus/matrix modulus) of 100.   For each shape of reinforcement, both the internal RVE and the boundary RVE were studied. Figs. 5.1 and 5.2 show the normal and tangential stress along the interfaces for the internal RVE, respectively. The stress values were normalized by the average normal stress of the circular shape reinforcement element. Figs. 5.3 and 5.4 show the same kind of stresses for the boundary RVE with the same normalization. The horizontal axis in the figures indicates the angle θ from the x-axis along the interface as illustrated in Figure 4.1.

For all cases, the normal stress was greater than the tangential shear stress at the interface in terms of the magnitude. For a reinforcement shape with a sharp corner(s), there was a stress concentration as expected. (These high stress values may not exist as the corner becomes rounded.) Other than the stress concentration at corners, the normal stress was larger around the upper section of the interface (i.e. near $\theta=90$) and it was a tensile stress as expected. The normal stress was in compression at the interface section close to the x-axis (i.e. $\theta=0$) for the internal RVE because the Poisson's ratio of the matrix material was greater than that of the reinforcing material. For the boundary RVE, on the other hand, the interface normal stress close to the x-axis almost vanished because of the traction-free boundary effect.

25

For reinforcement in a polygonal shape like square, octagon, diamond, the normal stress distribution was approximately constant along each linear segment of interface for the internal RVE except for the corner effect. The normal stress level increased from compression to tension as each linear segment became farther from the horizontal axis. Thus, the square shape reinforcement resulted in a two-step variation of normal stress, and the octagonal shape yielded a three-step variation. The diamond shape had an approximately constant stress variation except for two corner regions. Therefore, as the number of linear segments increases, the normal stress distribution is expected to approach to the normal stress distribution of circular reinforcement.

Among the four different shapes, the square shape had the largest tensile normal stress even not including stress concentration so that it might have a greater chance of interface debonding compared to other shapes. More detailed discussion for debonding is given in the next chapter. The circular and diamond shapes had lower normal stresses (except for the two corner zones in the diamond shape) compared to others. This implies that those shapes may have a less chance for interfacial debonding.

The interface stresses in the boundary RVE were generally lower than those in the internal RVE. For example, the normal stress for the square reinforcement was about 50 percent greater for the internal RVE, and approximately 25 percent for other shapes. It is expected that interface debonding may occur inside of a composite rather than at the boundary of the composite. For the boundary RVE, the normal stresses for polygonal shapes also show stepwise distributions along the interfaces, and they were almost negligible on the interface elements located from $\theta=0$ to about 45 except for the square shape of reinforcement that has stress rise at the corner.

The shear stresses vanished at $\theta=0$ and 90 for all shapes except for the diamond. For the internal RVE, the shear stress distribution is quite symmetric about $\theta=45$, while it is unsymmetrical for the boundary RVE and has a shift toward $\theta=90$. If the stress concentration cites were neglected, the peak shear stresses for four different shapes would be close to each other.

B.   VOLUME FRACTIONS

For the present analysis, only the circular shape reinforcement was used for different volume fractions. The reinforcement volume fraction varied from 20% to 70%. In addition, three different shear modulus ratios between the reinforcing material and the matrix material were considered and they were G_r/G_m=10, 100, or 1000, where G denotes the shear modulus and the subscripts r and m indicate the reinforcing and matrix materials, respectively. The reason for using shear modulus ratios instead of elastic modulus ratios was because the shear modulus values were used directly for the BEM calculations even though elastic and shear moduli were related to each other with a known Poisson's ratio. For the different volume fraction calculations, the results were calculated for the same Poisson's ratios.

Normal and tangential stresses along the interface were calculated and the results were plotted for different volume fractions and shear modulus ratios in Figs. 5.5, 5.6, 5.7, 5.11, 5.12 and 5.13 for internal RVE, and 5.8, 5.9, 5.10, 5.14, 5.15 and 5.16 for boundary RVE. The stresses were normalized by the average normal traction values along the boundary of their own where boundary conditions were applied.

For the uniform displacement boundary condition equivalent to a unit average traction along the boundary, Figure 5.5 shows that the reinforced composite has almost the same normal interface stress distribution regardless of the reinforcement volume fraction if the shear modulus ratio between the reinforcing and matrix materials is not high for internal RVE (i.e. G_r/G_m=10). For the boundary RVE, the results are close to each other but not as much like as in internal RVE. As the shear modulus ratio increases to 100 and higher as shown in Figs. 5.6 and 5.7 for internal RVE, and in Figs. 5.9 and

5.10 for boundary RVE, the interface normal stress variation becomes different for different reinforcement volume fractions for both internal and boundary RVEs. A higher volume fraction shows a greater fluctuation in the normal stress and a higher tensile stress values at the interface of around $\theta=90$. As long as the shear modulus ratio is about 100 or higher, the normal stress is almost independent of the modulus ratio. (See the comparison between Figs. 5.6 and 5.7, and between 5.9 and 5.10).

For internal RVE, the interface shear stress shows large variations among different reinforcement volume fractions with symmetric results about the interface at $\theta=45$. A lower reinforcement volume fraction results in a higher shear stress at the location at $\theta=45$. At 40% volume fraction, the shear stress shows a more or less flat plateau at the peak value. However, as the volume fraction becomes 60% or 70%, the stress plot shows double peaks as seen in Figs. 5.11 through 5.13. Like the normal stress, the shear stress is not affected by the shear modulus ratio as long as the ratio is about 100 or higher. Those are for the internal RVE.

For boundary RVE, the shear stress distribution is different for each volume fractions but not as much as those of internal RVE, and the results don't show symmetric distribution. The peak values are seen at about 55-75 degrees. Differently from internal RVE, 40% volume fraction shows the highest maximum tangential shear stress for all shear modulus ratios (See Figs. 5.14, 5.15 and 5.16). At higher shear modulus ratios, like internal RVE, the shear stress is not affected by the shear modulus ratios (Compare Figs. 5.15 and 5.16).

C.   EFFECTIVE ELASTIC MODULUS

In this section, the effective composite elastic moduli were computed for different shapes and volume fractions of reinforcements. Figs. 5.17 and 5.18 plot the normalized effective modules as a function of the reinforcement volume fraction for different ratios of the shear moduli between the reinforcing and matrix materials. When the shear modulus ratio is 10, the effective modulus shows an approximately linear variation depending on the reinforcement volume fraction. However, as the shear modulus ratio becomes higher, the effective modulus variation becomes nonlinear for different volume fractions. In particular, the slope of the effective modulus variation gets greater as the volume fraction or the shear modulus ratio increases. When the Figs. 5.17 and 5.18 are compared, it is seen that the effective composite elastic modulus values for the internal RVE are greater than those of boundary RVE. As the shear modulus ratios between reinforcing and matrix material increase, the difference between the internal and boundary effective composite moduli gets higher.

The effective elastic moduli for four different shapes with G_r=1000, G_m=10, v_r=0.3, v_m=0.49, and 40% reinforcement volume fraction were listed in Table 1:

Table 1. The effective composite elastic modulus results for four different shapes.

E_{eff}	Square	Octagonal	Circular	Diamond
Boundary RVE	4.8374	3.6018	3.4639	3.4379
Internal RVE	6.9787	4.9773	4.7242	4.7146

As seen from the results, in general they are higher for internal RVE, and square shape reinforcement element gives the highest results among them for both internal and boundary RVEs, and the circular and the diamond shapes gives the lowest.

Because there was a big difference between the square shape and others in terms of the effective moduli, the four shapes were analyzed for a case with known experimental data [Ref. 7]. This time, G_r=29.96 GPa., G_m=1.28 GPa., v_r=0.22, v_m=0.35, and 40% reinforcement volume fraction were used, and the results are listed in the table 2. The results were calculated for both internal and boundary RVEs as well as using other analytical models [Refs. 8 and 9]. As seen from Table 2, the results for four different shapes were a little higher than those of other data for both internal and boundary RVEs. The internal RVE results are between 6-8% higher than boundary RVE results. The boundary RVE results are closer to the other data.

From Table 1, it was observed that the square shape reinforcement gave a 35-40% greater effective modulus than other shapes. However, Table 2 shows more comparable values between the square and other shapes. In order to identify what causes this difference in Table 1, five different cases were studied at different shear moduli and Poisson's ratios and the results were tabulated in Table 3. In the table, for the same shear modulus ratios (G_r=1000, G_m=42.72), higher Poisson's ratios for reinforcing and matrix material give much higher effective elastic modulus values for the square shape. On the other hand, when the Poisson's ratios of both material remained the same ($v_r = 0.22, v_m = 0.35$), different shear modulus ratios give very close effective elastic moduli for the four shapes. Another comparison was made by taking the Poisson's ratio of one material constant and decreasing the other material's Poisson's ratio. When the

Poisson's ratio of the matrix material was constant (v_m=0.49), the decrease in reinforcing material from 0.30 to 0.22 gives very small different results, about 1% difference. However, when the Poisson's ratio of reinforcing material was constant (v_r=0.30), the decrease in matrix material from 0.49 to 0.45 gives quite different results, about 15-25% less than the first results. This result concludes that the Poisson's ratio of matrix material plays a critical role for the effective composite elastic modulus. For all the cases listed in Tables 1, 2, and 3, the effective elastic moduli for the square shape reinforcement were higher than other shapes' values. When the x and y traction values for the interface elements were examined, it is seen that the overall traction values in the x direction for square shape were higher than the other shapes' values for the same shear modulus and Poisson's ratio values. This means that the square shape reinforcement resists to the shrinking matrix material with a higher stress value than the other shapes. This causes a counter effect of Poisson's effect, and makes the composite material stiffer. In Table 3, although the shear modulus ratios and Poisson's ratios are different from each other, the effective elastic moduli for four different shapes coincide with the results in the study conducted by Shen, Finot, Needleman and Suresh [Ref. 2] in the qualitative sense. Their study used particle reinforcement rather than fiber reinforcement. Thus, it can be stated that the particle or fiber reinforcement give the same results qualitatively.

32

Table 2. The comparison of four shapes with different formulation for 40% reinforcement volume.

Composite Elastic Modulus (E_C) (Gpa)	G_r=29.96, G_m=1.28 $v_r = 0.22, v_m = 0.35$ (Boundary RVE)	G_r=29.96, G_m=1.28 $v_r = 0.22, v_m = 0.35$ (Internal RVE)
Experimental Results 2nd order [Ref. 7]	7.3247	7.3247
Kwon Results [Ref. 8]	7.6375	7.6375
Circular shape	8.0523	8.5439
Diamond shape	8.5294	9.2564
Square shape	8.7975	9.3516
Octagonal shape	8.1386	8.7916
Analytical results [Ref. 10]	6.7587	6.7587

Table 3. The comparison of four different shapes at different shear modulus ratios and at different Poisson's ratios.

E_{eff}	Square	Octagonal	Circular	Diamond
G_r=1000 G_m=42.72 v_r=0.30, v_m=0.49	5.1931	4.1690	4.0332	3.9464
G_r=1000 G_m=42.72 v_r=0.22, v_m=0.49	5.1194	4.1314	3.9997	3.8980
G_r=1000 G_m=42.72 v_r=0.30, v_m=0.45	3.9124	3.3836	3.3121	3.3678
G_r=1000 G_m=42.72 v_r=0.22, v_m=0.35	2.4945	2.3144	2.2890	2.4250
G_r=1000 G_m=10 v_r=0.22, v_m=0.35	2.7704	2.4984	2.4651	2.6799

D. THE STRES AND EFFECTIVE ELASTIC MODULUS RESULTS FOR DOUBLE REINFORCEMENT CASE

Finally, a double circular reinforcing case was studied without debonding. For this analysis, two circular shape reinforcement materials that had equal volume fractions, 20% each, and different volume fractions, 30% and 10%, were studied. The reinforcing material had again 40% total volume fraction. The same material properties as before were used in this study. For the same boundary condition, normal and tangential stresses along the interfaces were calculated and the results were plotted for each interface of the unit cell separately. Figs. 5.19 and 5.20 plot the normal stresses normalized in terms of the average normal traction values along the boundary caused by the applied uniform displacement. It is observed that the equal size reinforcement case gave an almost linear variation of the normal stress along the interface. For different shear modulus ratios, the results were the same. In addition, the results for both interfaces were the same as expected from symmetry. For the different sizes of reinforcement case, the normal stress was much higher on the interface of the larger particle than on the interface of the smaller reinforcement. Not only the magnitude but also the shapes of the normal stress distribution were very different between the two different sizes of reinforcement. It is to be noted that the normal stress along the smaller reinforcement was almost zero if $G_r/G_m=10$. The peak stress value for the non-uniform particle sizes was almost twice greater than that for the uniform particle size. In Figs. 5.21 and 5.22, the normalized tangential stresses were plotted for equal and different sizes of reinforcement cases respectively. In Figure 5.21, the equal size reinforcement case gave the same results for both interfaces, and for different shear modulus ratios the results were close to each other. For the different sizes of reinforcement case, the results for different shear modulus ratios

34

were quite different from one another. Again the non-uniform sizes of reinforcement gave much higher stresses than the uniform size. Like the previous stress distributions, the larger reinforcement in the non-uniform sizes of reinforcement case gave the highest shear stress values.

Finally, the effective elastic moduli were calculated for each case with three different shear modulus ratios. The effective moduli were normalized by the elastic moduli of the matrix material. The results were tabulated in Table 4. As seen from the table, the normalized effective elastic moduli is the highest for $G_r/G_m=100$ among others. However, the non-normalized effective modulus increases along with the increasing reinforcement shear modulus as expected. As seen from Tables 1 and 4, the elastic modulus for the single reinforcement of circular shape is greater than those for double reinforcement cases. Furthermore, different sizes of reinforcement resulted in a smaller effective modulus than the same size of reinforcement. These results coincide with the results conducted by Shen, Finot, Needleman and Suresh [Ref. 2].

Table 4. The normalized elastic modulus values for double reinforcement cases.

E_{eff} (E_c/E_m)	$G_r/G_m=10$	$G_r/G_m=100$	$G_r/G_m=1000$
$R_1=0.5046$, $R_2=0.5046$ (20% each)	2.1644	2.3892	2.2819
$R_1=0.6180$, $R_2=0.3568$ (30% +10%)	2.0870	2.2359	2.0503
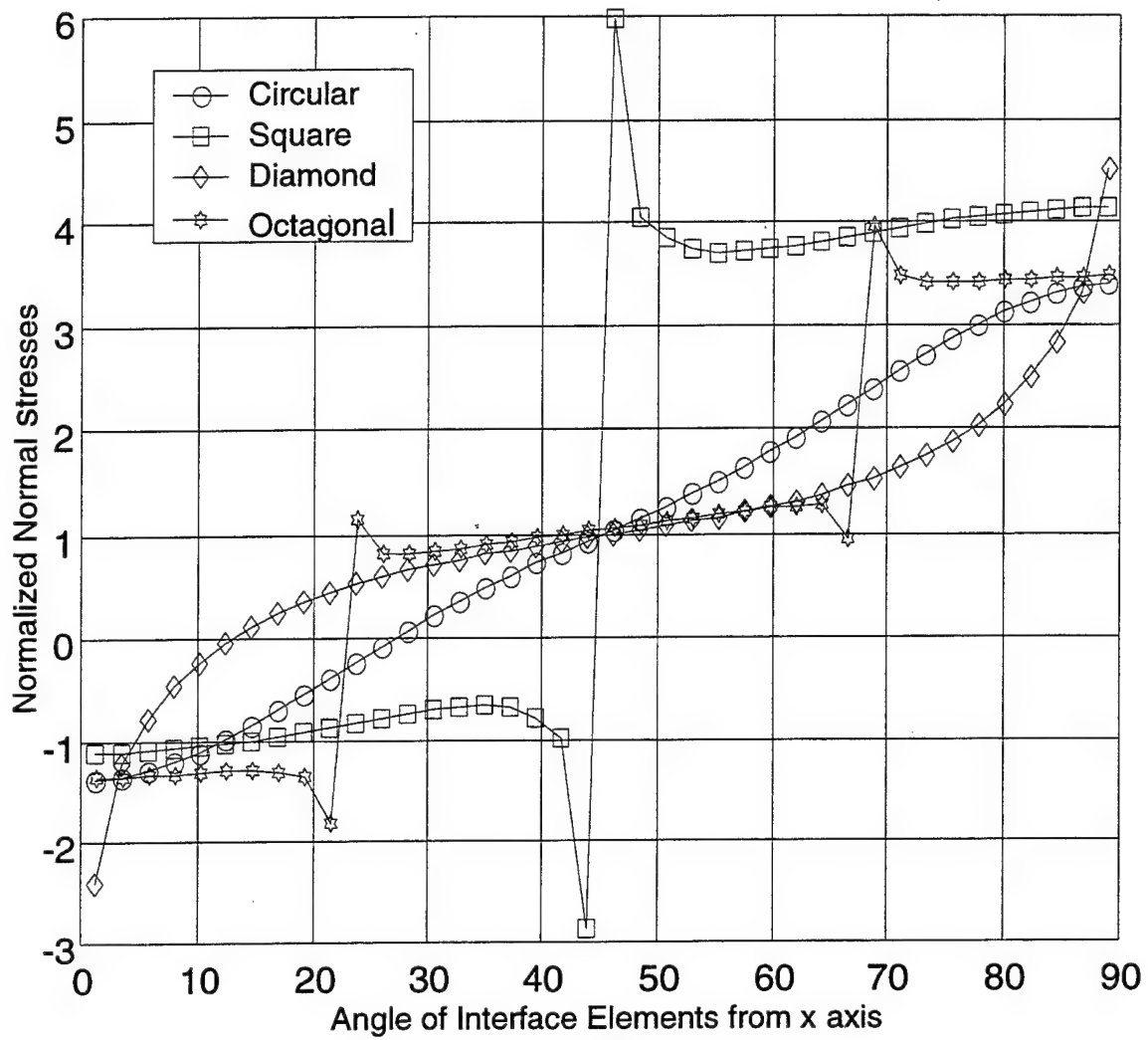
Figure 5.1: The Normal Stresses Along the Interfaces of Different Shapes, Normalized by Average Normal Stress of Circular Shape Reinforcement for Internal RVE $(G_r/G_m=100)$.
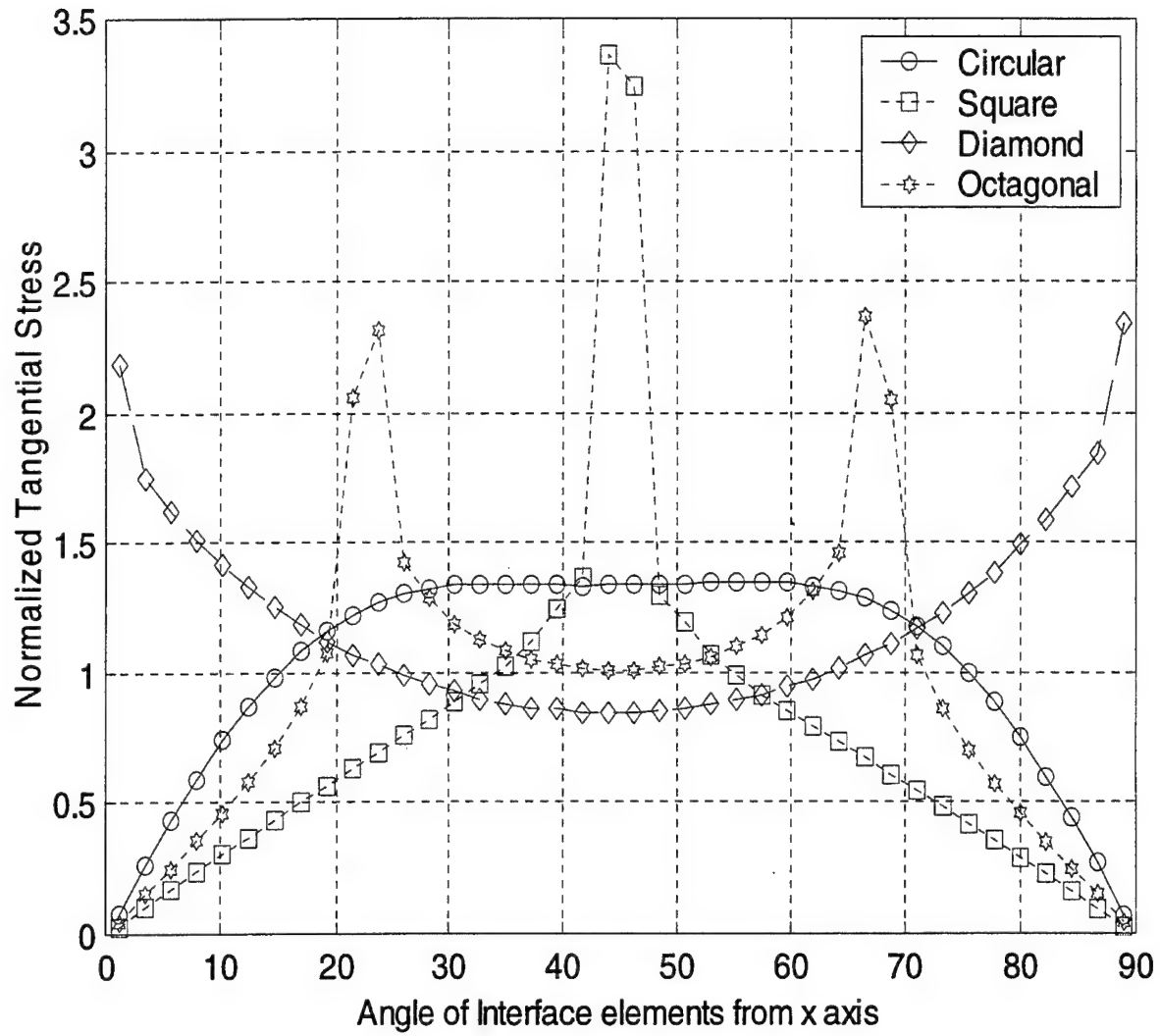
Figure 5.2: The Tangential Stresses Along the Interfaces of Different Shapes, Normalized by Average Normal Stress of Circular Shape Reinforcement for Internal RVE $(G_r/G_m=100)$.
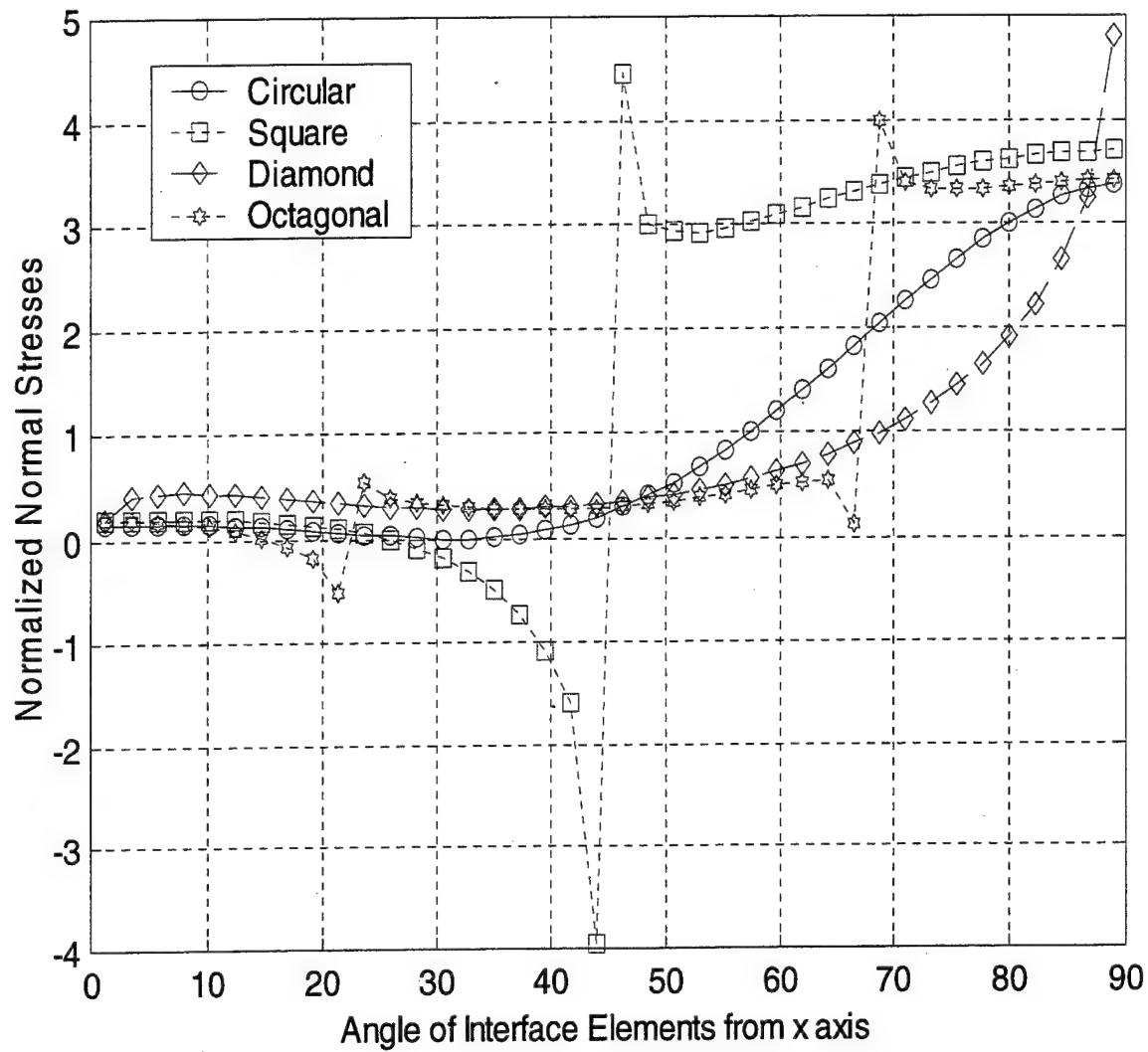
Figure 5.3: The Normal Stresses Along the Interfaces of Different Shapes, Normalized by Average Normal Stress of Circular Shape Reinforcement for Boundary RVE $(G_r/G_m=100)$.
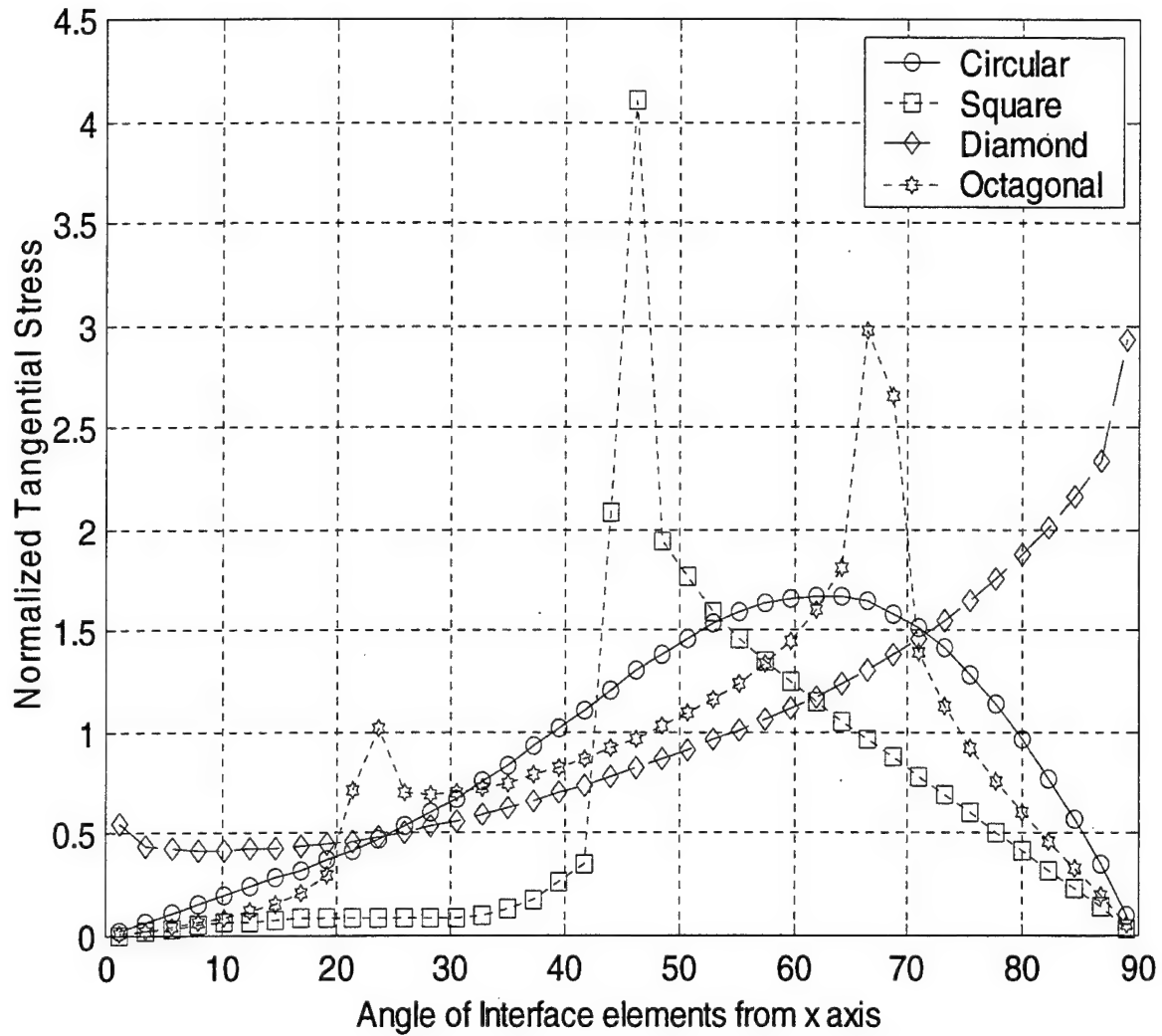
Figure 5.4: The Tangential Stresses Along the Interfaces of Different Shapes, Normalized by Average Normal Stress of Circular Shape Reinforcement for Boundary RVE ($G_r/G_m=100$).
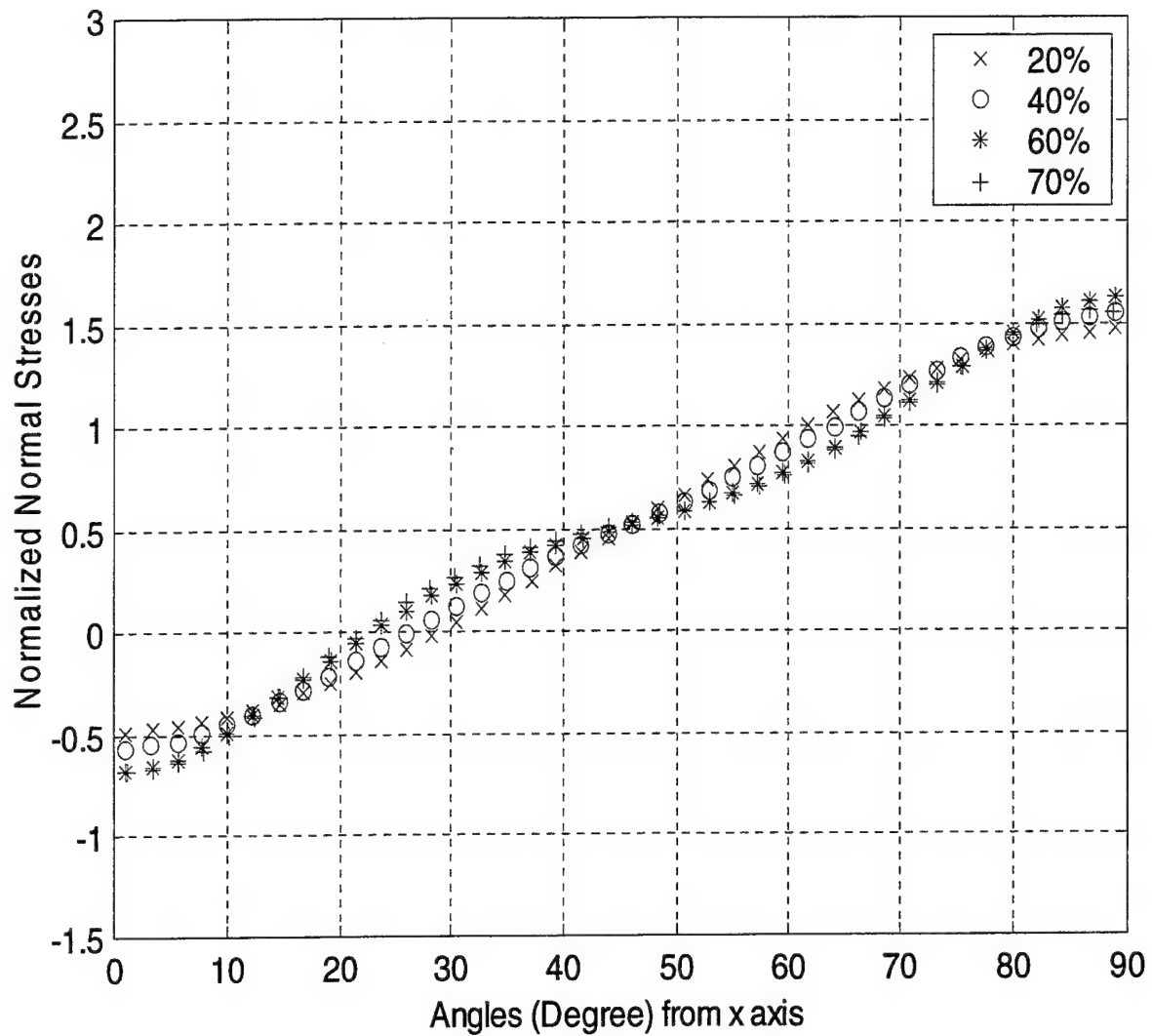
Figure 5.5: The Normal Stresses Along the Interfaces of Four Different Volume Fractions Normalized by the Average Normal Stress Values Along the Boundaries of Their own where Boundary Conditions were Applied, for Internal RVE (Gr/Gm=10).
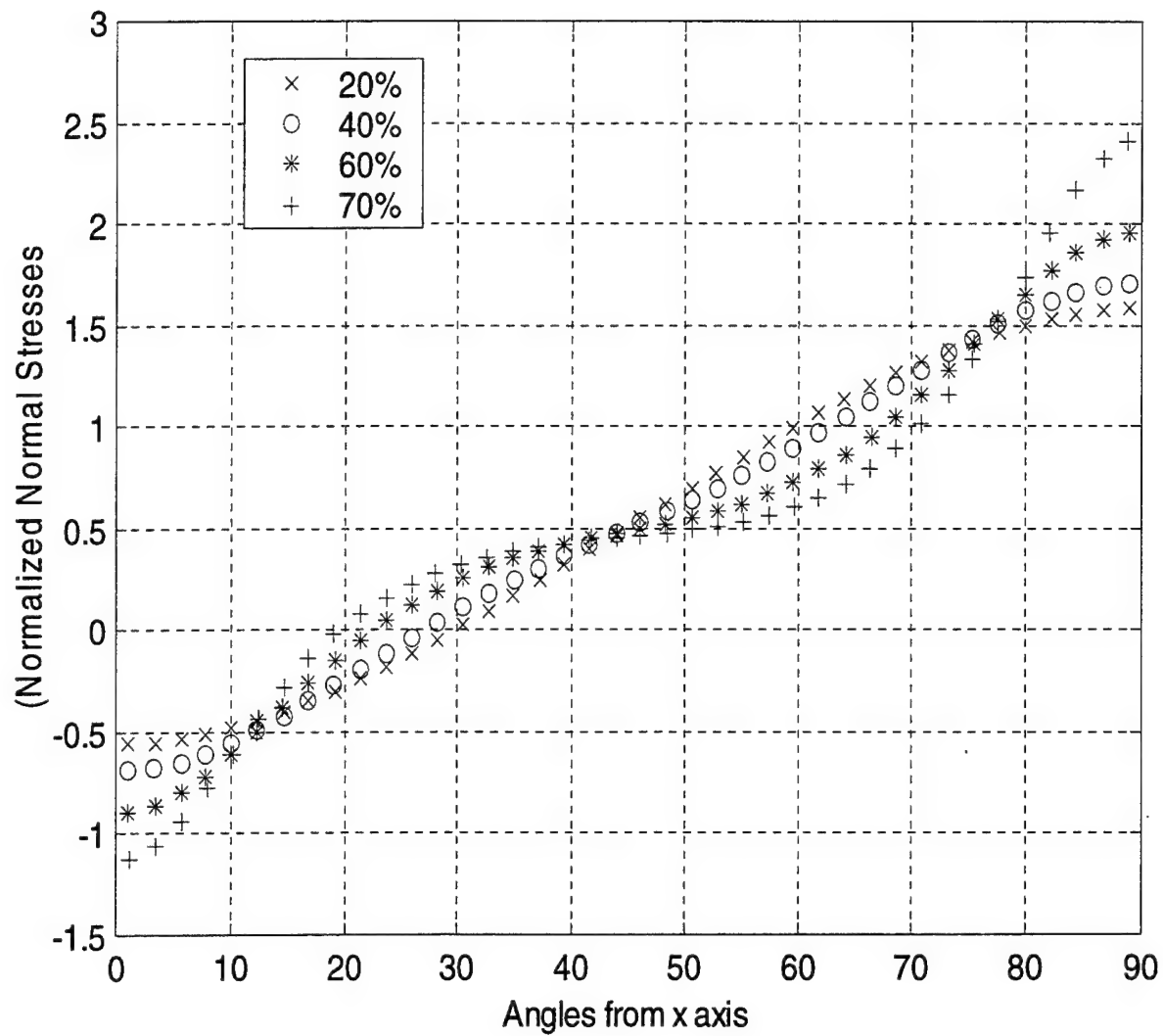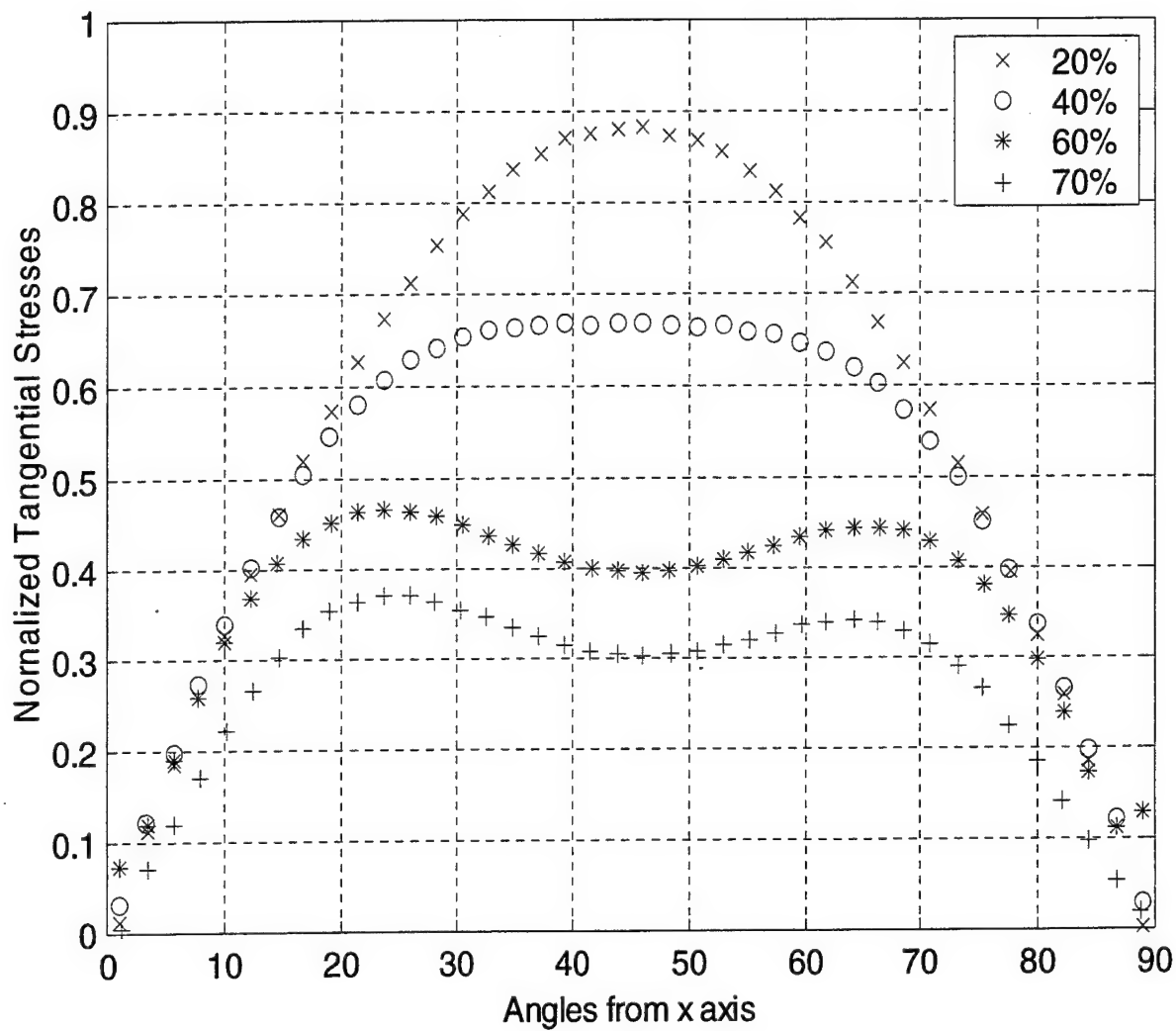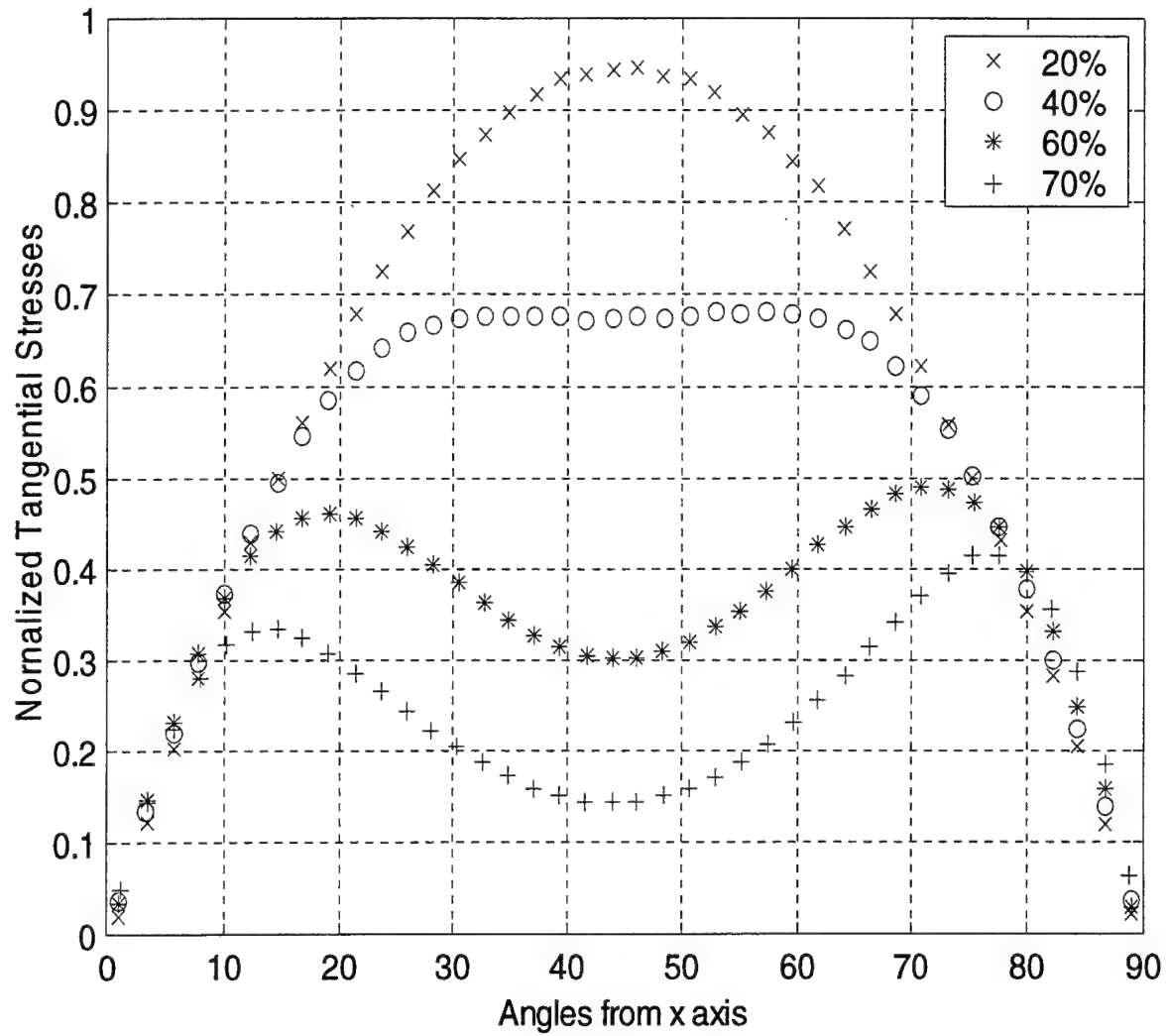
Figure 5.6: The Normal Stresses Along the Interfaces of Four Different Volume Fractions Normalized by the Average Normal Stress Values Along the Boundaries of their own where Boundary Conditions were Applied, for Internal RVE (Gr/Gm=100).
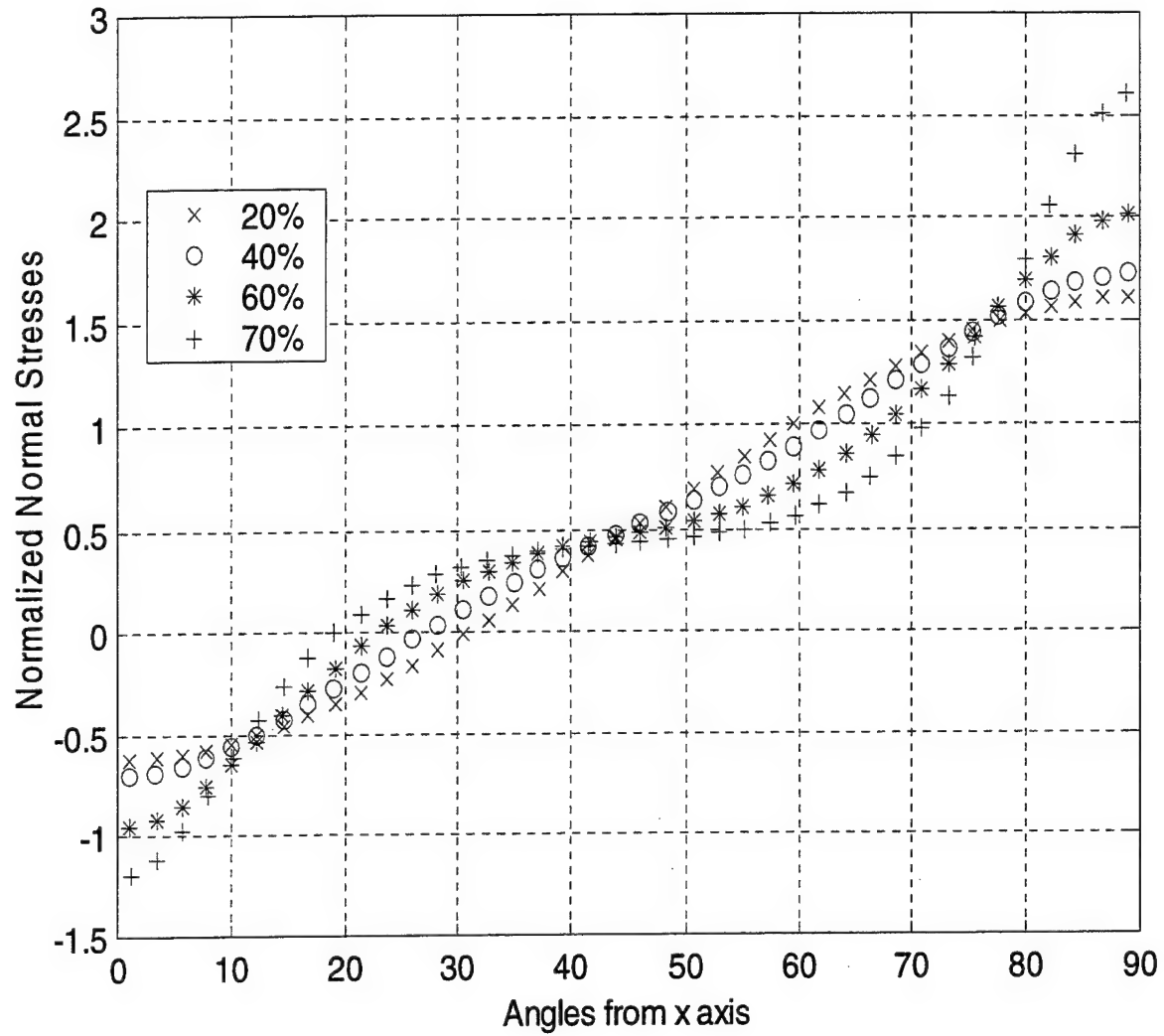
Figure 5.7: The Normal Stresses Along the Interfaces of Four Different Volume Fractions Normalized by the Average Normal Stress Values Along the Boundaries of their own where Boundary Conditions were Applied, for Internal RVE (Gr/Gm=1000).
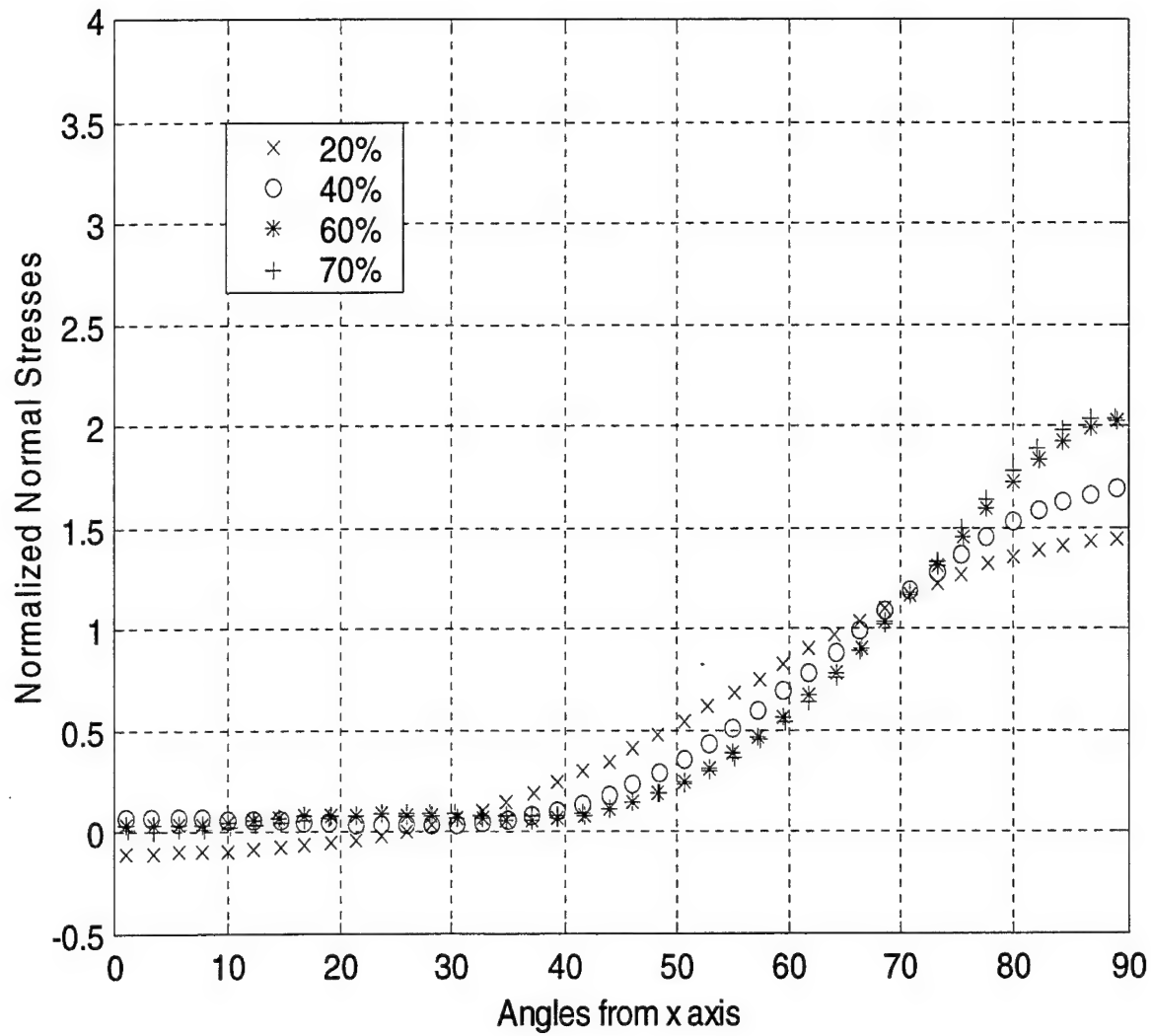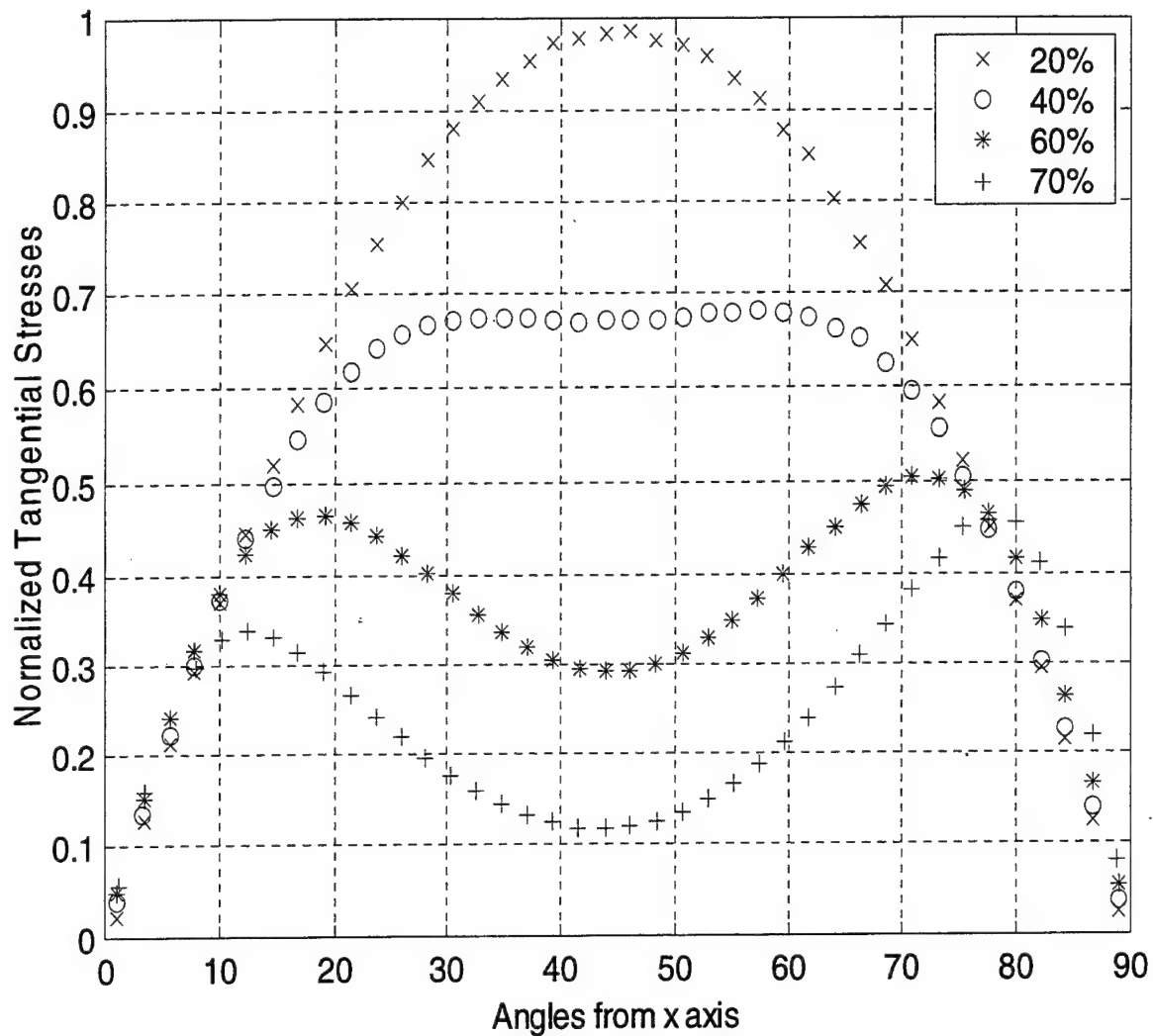
Figure 5.8: The Normal Stresses Along the Interfaces of Four Different Volume Fractions Normalized by the Average Normal Stress Values Along the Boundaries of their own where Boundary Conditions were Applied, for Bboundary RVE (Gr/Gm=10).
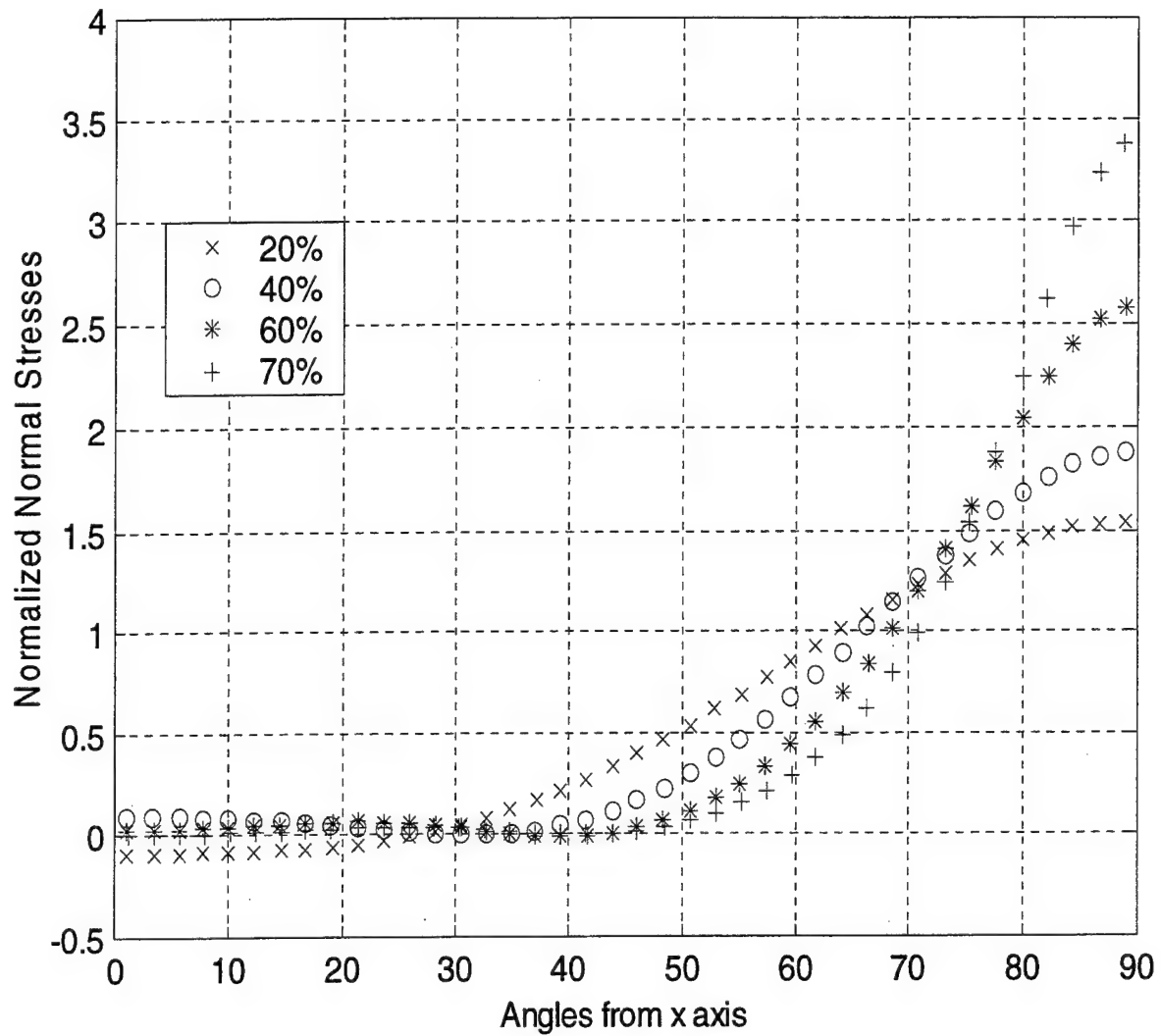
Figure 5.9: The Normal Stresses Along the Interfaces of Four Different Volume Fractions Normalized by the Average Normal Stress Values Along the Boundaries of their own where Boundary Conditions were Applied, for Boundary RVE (Gr/Gm=100).
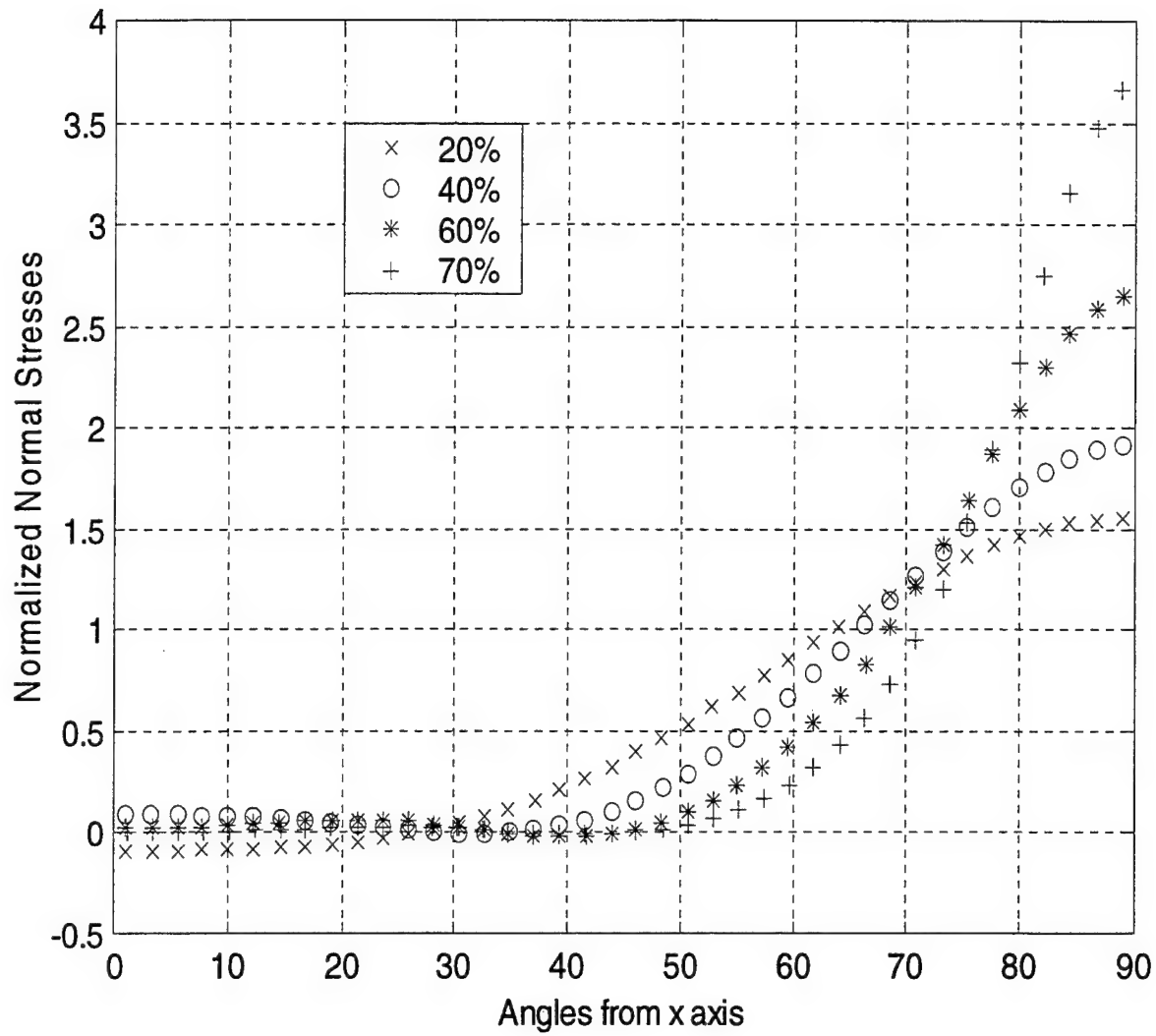
Figure 5.10: The Normal Stresses Along the Interfaces of Four Different Volume Fractions Normalized by the Average Normal Stress Values Along the Boundaries of their own where Boundary Conditions were Applied, for Boundary RVE (Gr/Gm=1000).
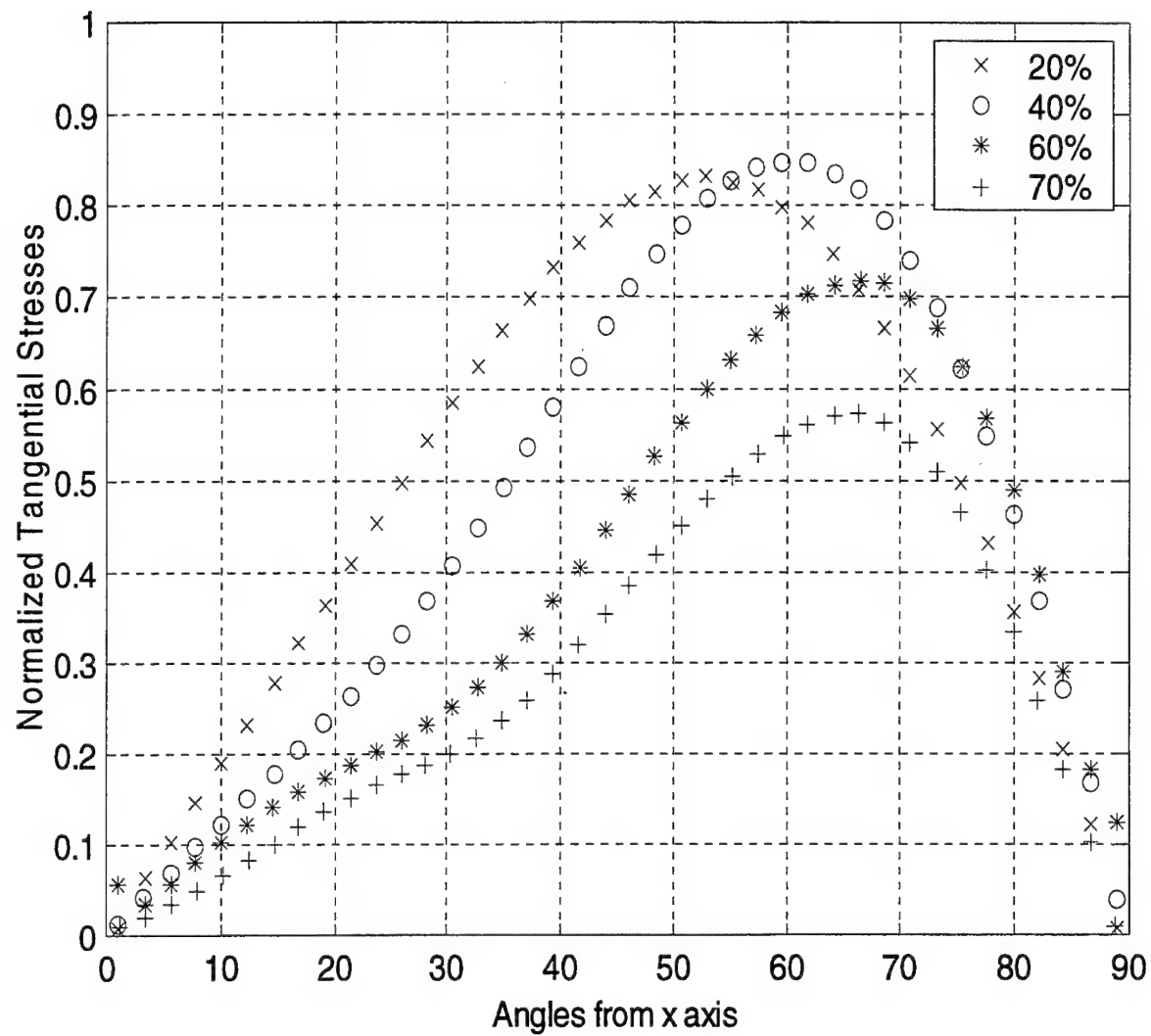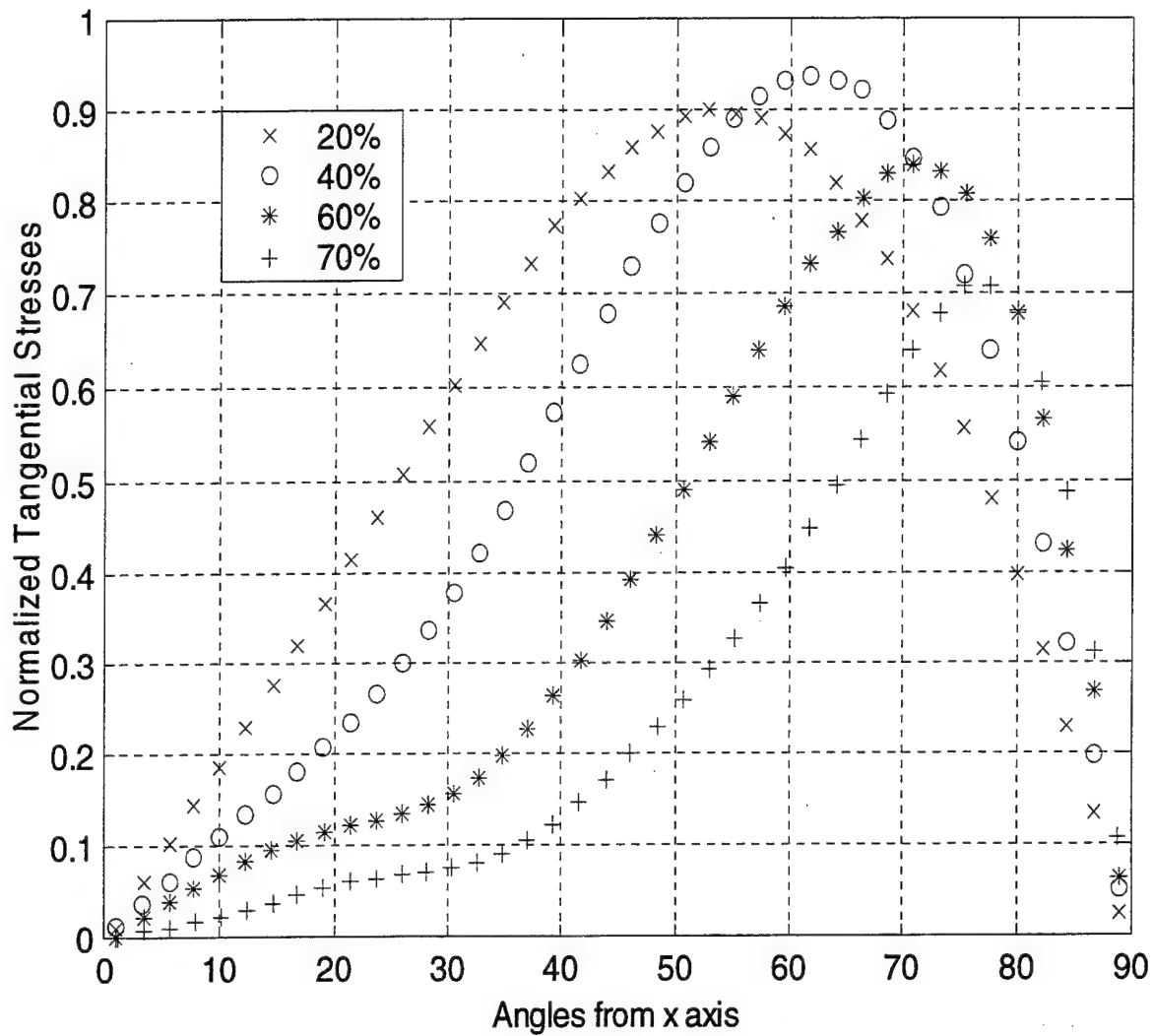
Figure 5.11: Tangential Stresses Along the Interfaces of Four Different Volume Fractions Normalized by Average Normal Stresses Along the Boundary of each where Boundary Conditions were Applied for Internal RVE (Gr/Gm=10).
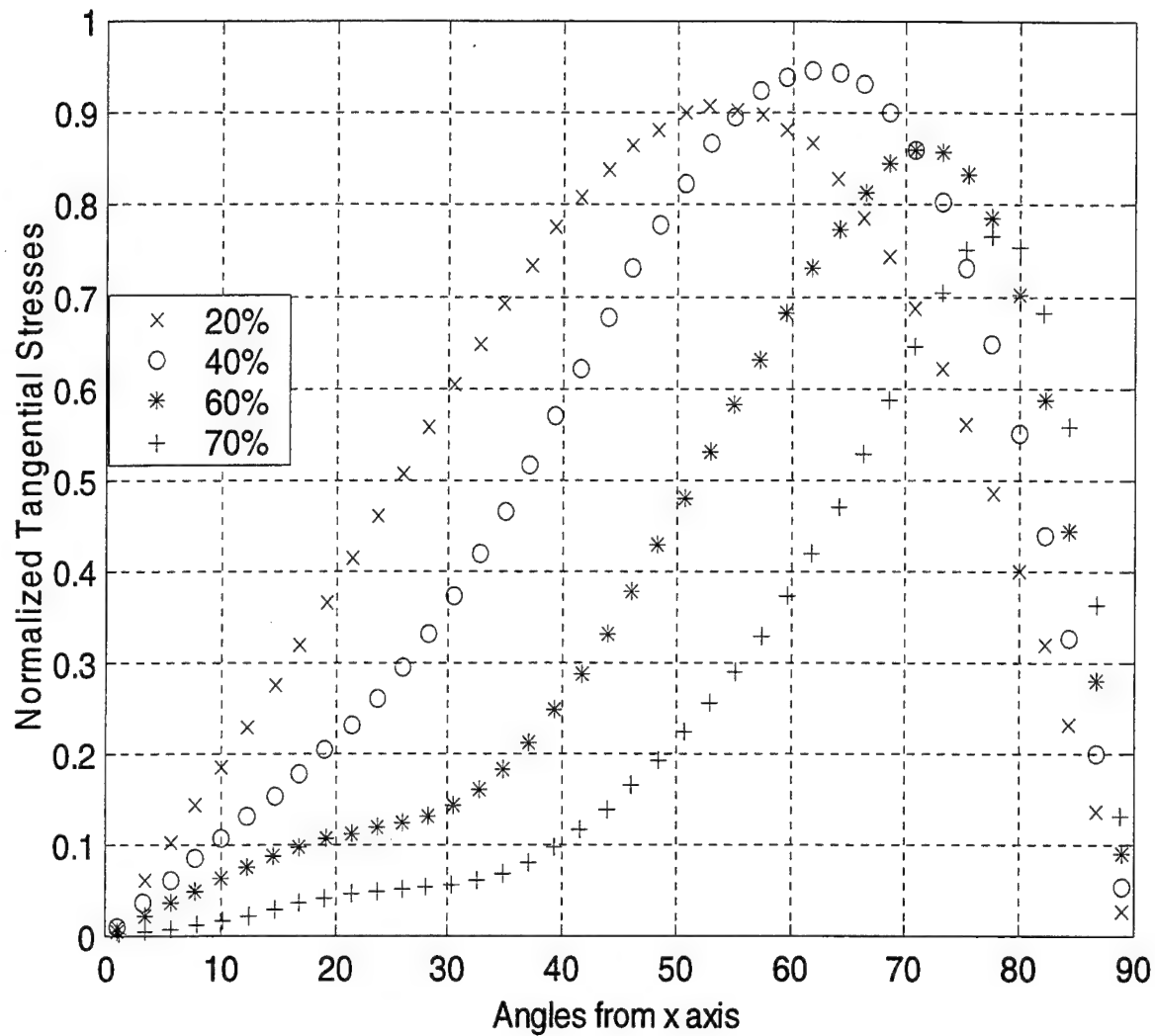
Figure 5.12: Tangential Stresses Along the Interfaces of Four Different Volume Fractions Normalized by Average Normal Stresses Along the Boundary of each where Boundary Conditions were Applied for Internal RVE (Gr/Gm=100).

Figure 5.13: Tangential Stresses Along the Interfaces of Four Different Volume Fractions Normalized by Average Normal Stresses Along the Boundary of each where Boundary Conditions were Applied for Internal RVE (Gr/Gm=1000).

Figure 5.14: Tangential Stresses Along the Interfaces of Four Different Volume Fractions Normalized by Average Normal Stresses Along the Boundary of each where Boundary Conditions were Applied for Boundary RVE (Gr/Gm=10).

Figure 5.15: Tangential Stresses Along the Interfaces of Four Different Volume Fractions Normalized by Average Normal Stresses Along the Boundary of each where Boundary Conditions were Applied for Boundary RVE (Gr/Gm=100).

Figure 5.16: Tangential Stresses Along the Interfaces of Four Different Volume Fractions Normalized by Average Normal Stresses Along the Boundary of each where Boundary Conditions were Applied for Boundary RVE (Gr/Gm=1000).
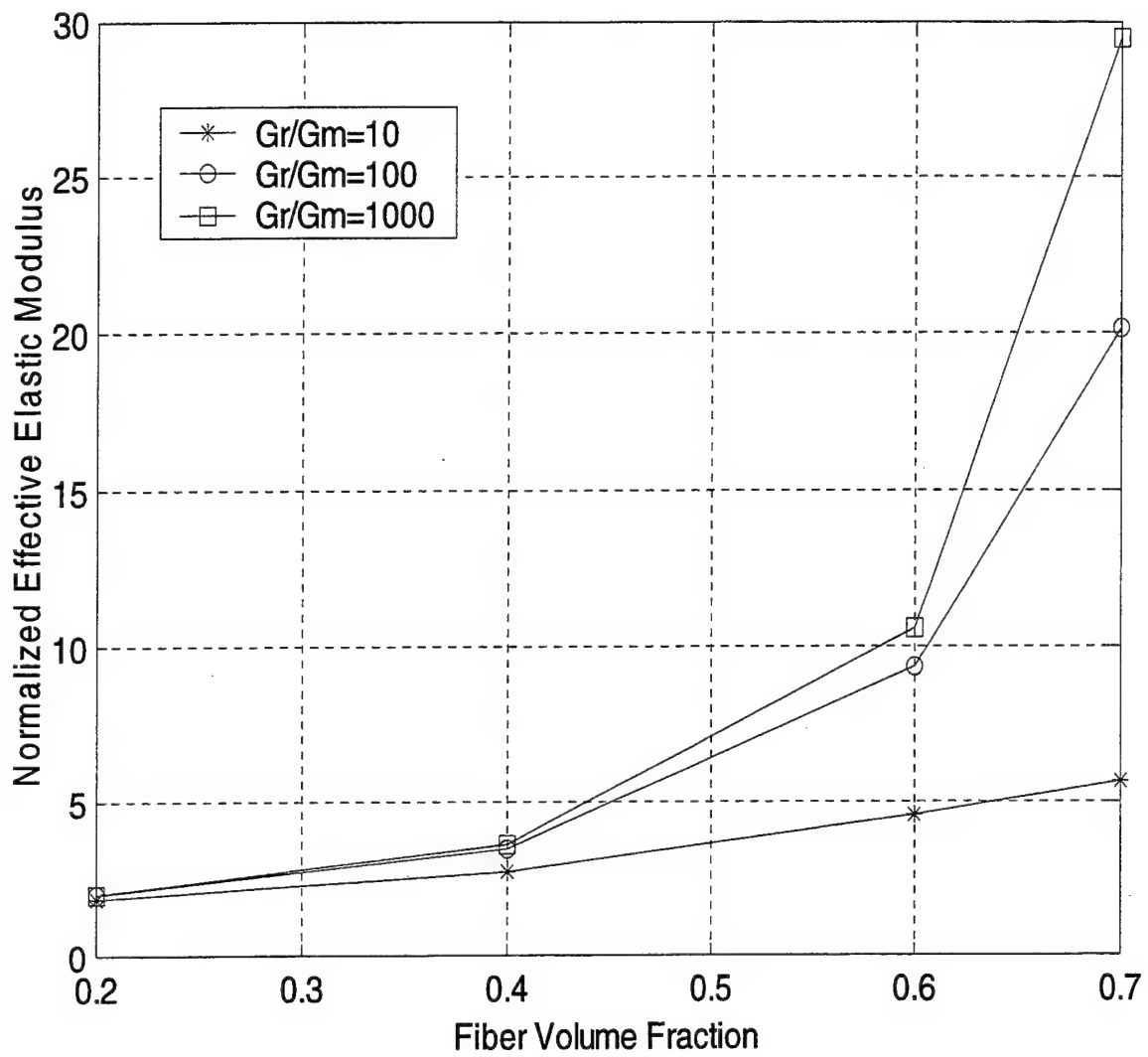
Figure 5.17: The Normalized Effective Elastic Modulus Values for Boundary RVE at Four Different Volume Fractions and Three Different Shear Modulus Ratios.
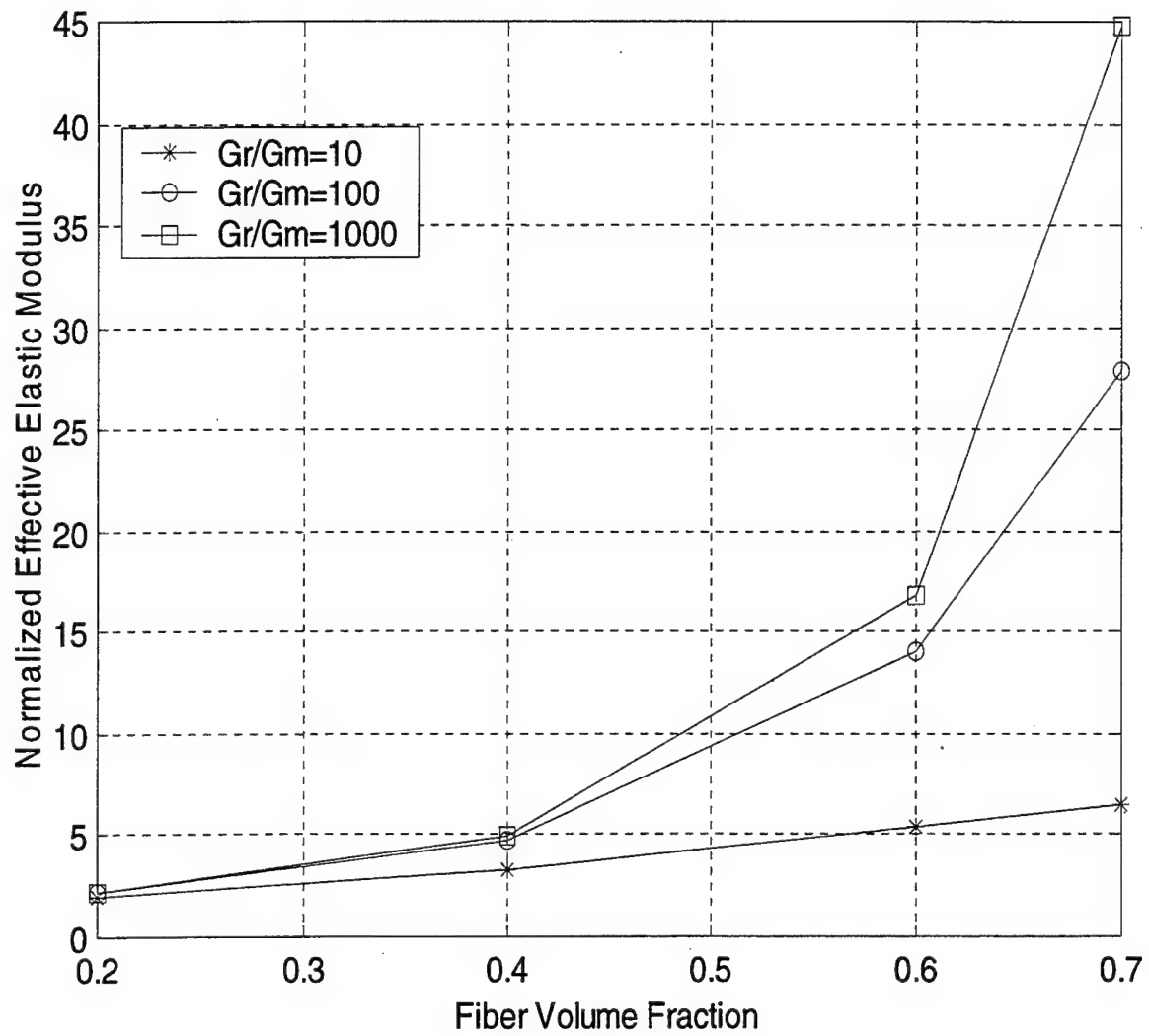
Figure 5.18: The Normalized Effective Elastic Module Values for Internal RVE at Four Different Volume Fractions and Three Different Shear Modulus Ratios.
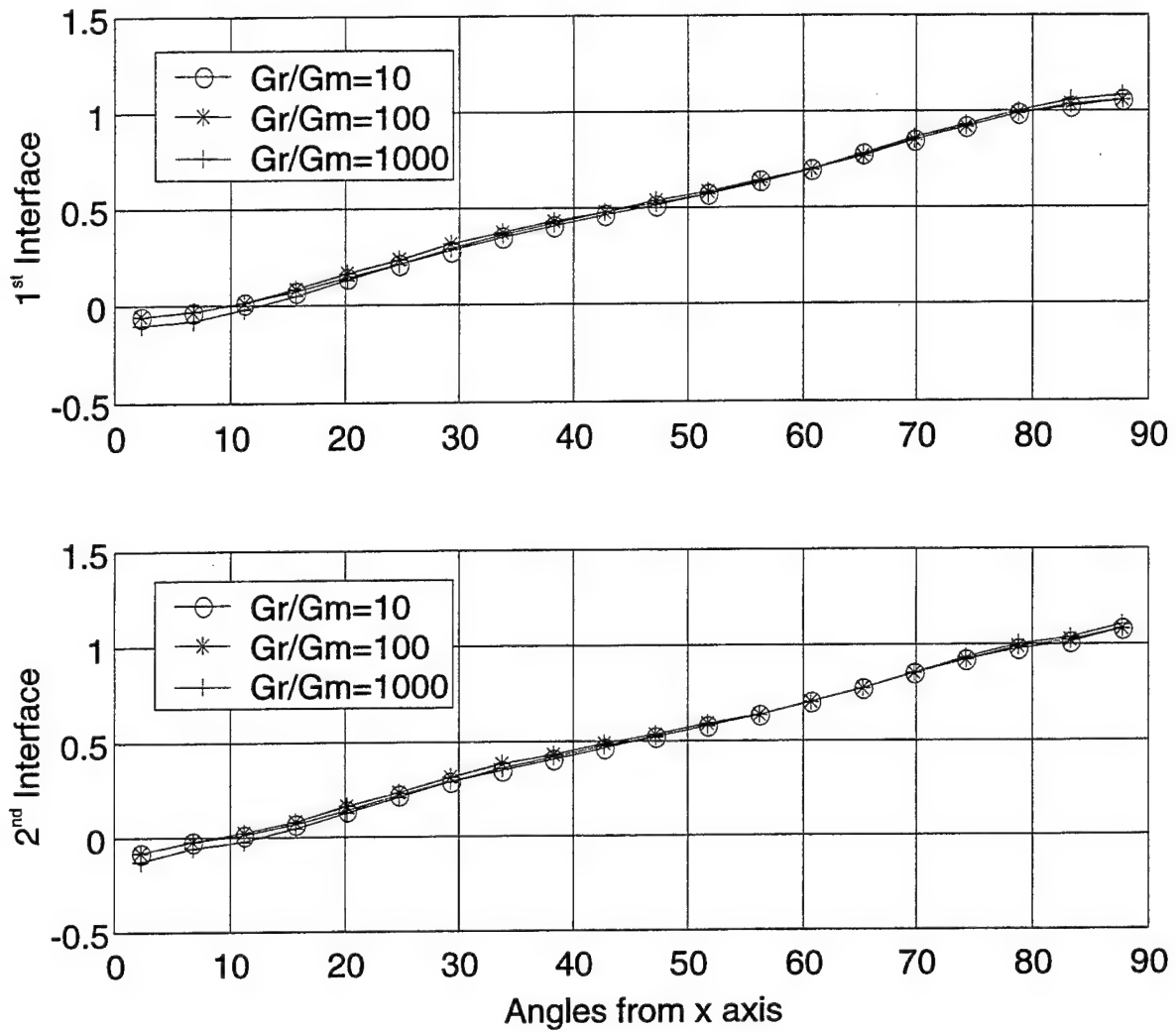
Figure 5.19: The Normalized Normal Stresses Along the Interfaces for Equal Size Reinforcement Elements (20% each) at Three Different Shear Modulus Ratios.
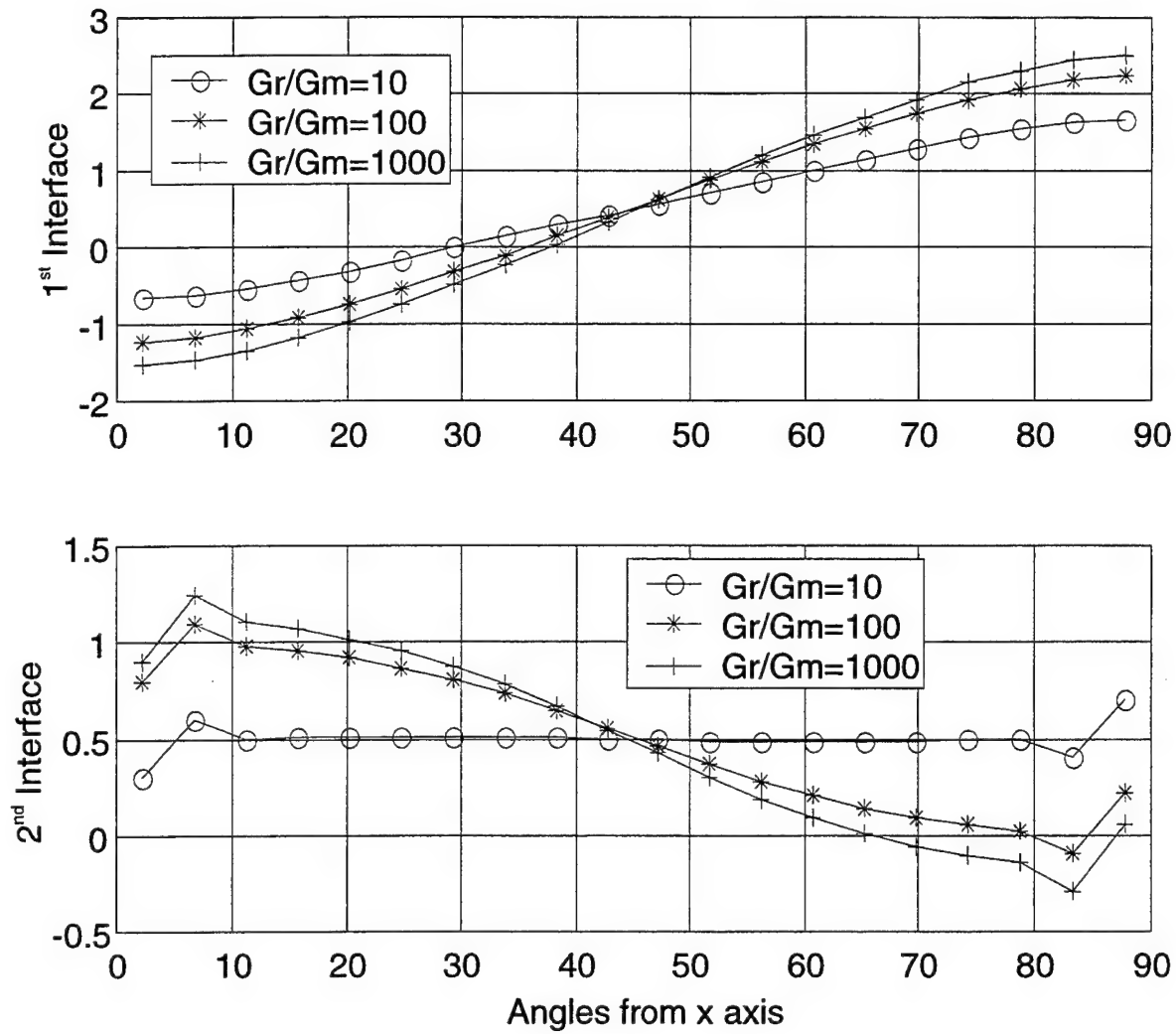
Figure 5.20: The Normalized Normal Stresses Along the Interfaces for Different Size Reinforcement Elements (30% and 10%) at Three Different Shear Modulus Ratios.
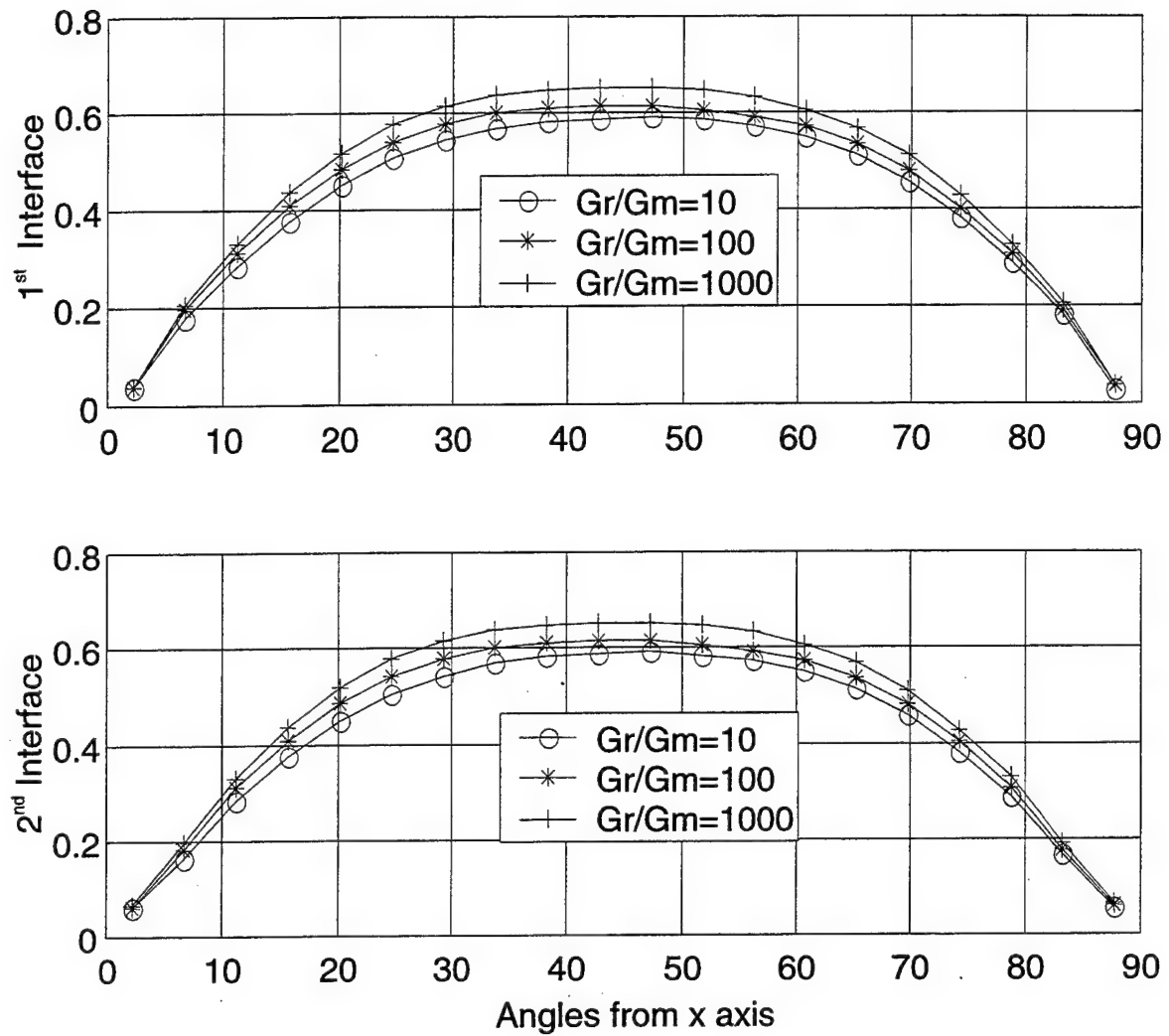
Figure 5.21: The Tangential Stresses at Average Unit Traction along the Interfaces for Equal Size Reinforcement Elements (20% each) at Three Different Shear Modulus Ratios.
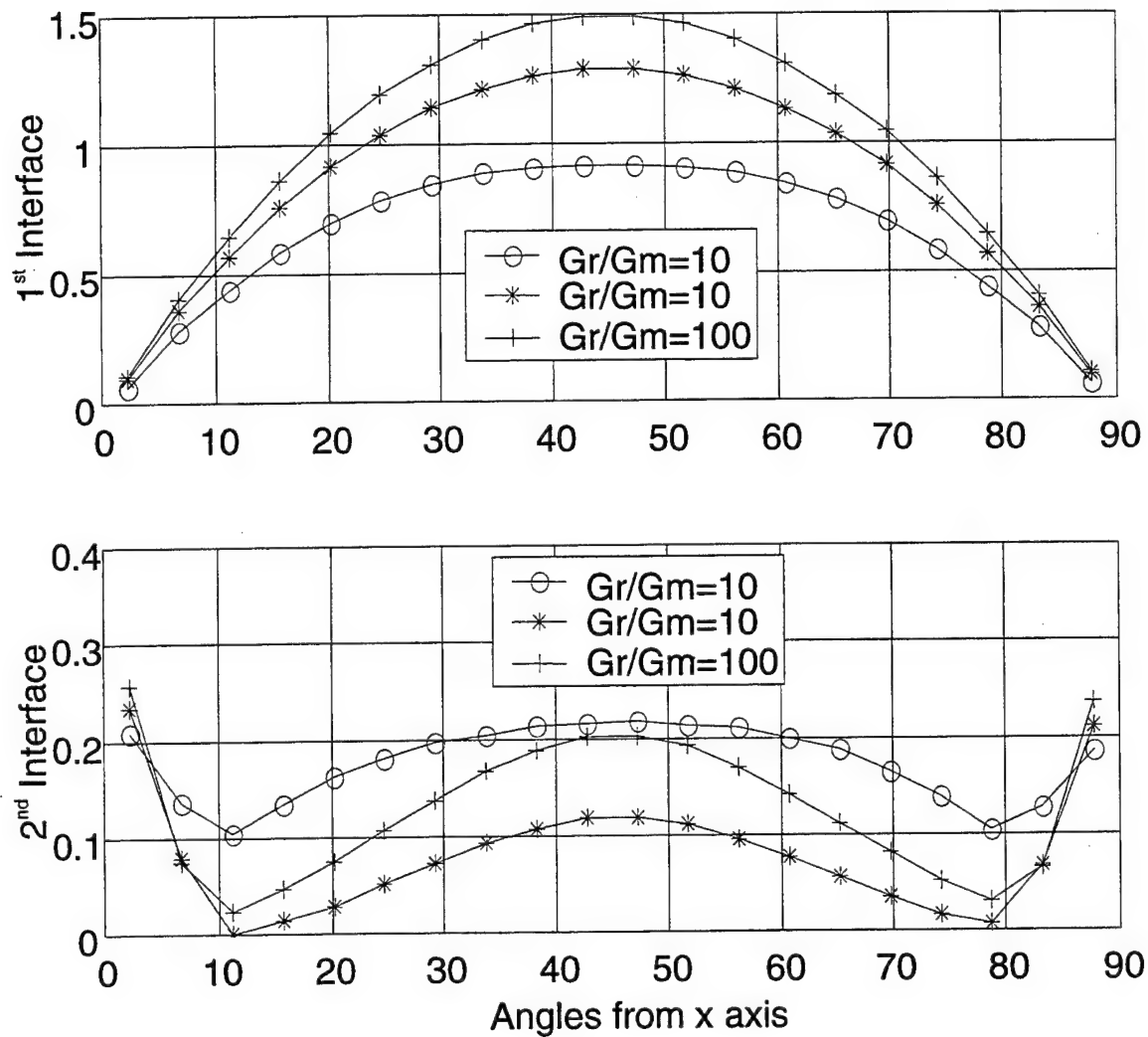
Figure 5.22: The Tangential Stresses at Average Unit Traction along the Interfaces for Different Size Reinforcement Elements (30% and 10%) at Three Different Shear Modulus Ratios.

THIS PAGE INTENTIONALLY LEFT BLANK

VI. RESULTS WITH INTERFACE DEBONDING

A. INTERFACE FAILURE CRITERIA

In the analysis of interface debonding, the Quadratic Failure Criterion [Ref. 10] was used as the failure criterion, which has been commonly used for composite materials. The Quadratic Failure Criterion is expressed below;

$$\left(\frac{\sigma_N}{S_N}\right)^2 + \left(\frac{\sigma_T}{S_T}\right)^2 \leq 1 \tag{6.1}$$

where σ_N and σ_T are normal and tangential stresses at the interface , S_N and S_T are the normal and tangential failure strength at the interface. The normal stress σ_N can be either tensile or compressive. Accordingly, proper normal failure strength S_N should be used depending on the status of the normal stress. In general, interface failure occurs much easily under tensile normal stress than compressive normal stress. That is, the normal strength S_N is much greater for compression than for tension. As a result, interface failure under compressive normal stress was not considered in this study. In addition, as an approximation, S_T is taken to be a half of S_N as usually assumed in a homogeneous isotropic material. Using this assumption, Equation 6.1 is transformed into

$$\sigma_{eq} = \sqrt{\sigma_N^2 + 4\sigma_T^2} \leq S_N \tag{6.2}$$

This expression has one strength value at the interface. The equivalent stress σ_{eq} was computed along the interface and progressive interface debonding was determined by the magnitude of the equivalent stress. In other words, interface debonding was assumed to occur at the location of the largest value of the equivalent stress. Once interface

debonding occurred, the debonded elements were assumed to be traction-free boundary elements assuming there was no friction at the interface after debonding. Then, the equivalent stress was recalculated and the previous process continued.

B. COMPARISON OF FAILURE STRESSES AND DEBONDING OF DIFFERENT REINFORCEMENT SHAPES

In the following study, the reinforcing material had a volume fraction of 40 percent and the shear modulus ratio of the reinforcement to the matrix material was 100. The failure criterion was also applied to four different shapes; circular, square, diamond and octagonal shapes. The equivalent stresses were plotted along their interfaces (See Figs. 6.1 and 6.2) for both internal and boundary RVEs.

From Figs. 6.1, and 6.2 , it is seen that, the sharp corners with stress concentration are the debonding initiation cites. It is also believed that even though the corners are more or less smooth as expected in a real composite, the stress at the corners are still greater or equal to the stresses at the rest of the interface. Those statements were the same for both internal and boundary RVEs.

Among the four shapes, the square shape of reinforcement had the highest chance of initiation of interface failure with or without stress concentration effect at the corner. The other three shapes showed close equivalent peak stress values except for the stress concentration. In other words, the three shapes might have initial interface failure under the almost same magnitude of the load if corners were smooth. Otherwise, the circular shape was the safest for interface failure initiation. When compared the internal RVE to the boundary RVE, the square shape indicated that interface failure initiation would occur at an internal location of a composite rather than at a boundary location. Other shapes showed a similar trend but the difference between internal and boundary RVEs was smaller than that for the square shape. Figure 6.3 shows the possible location of interface failure initiation and the direction of progressive failure for four different shapes.

After the initiation, it was observed that the debonding progressed along the neighboring horizontal and inclined interfaces until all these horizontal and inclined interfaces separated. The reason for this is, after every debonding, the stresses on the neighboring elements grow significantly and cause them to exceed the failure criterion until the debonding reaches the vertical interface elements of either square or octagonal shape. When the debonding reaches the vertical elements, the tensile stresses on these elements turn out to be compressive, and keeps the vertical elements from debonding due to Poisson's ratio effect, which is greater in matrix element than reinforcement element. Consequently, square shape reinforcement element will have maximum 50 percent and octagonal shape reinforcement element will have maximum 75 percent debonding (See Figs. 6.4 and 6.5). This situation is different for diamond and circular shape reinforcement elements. Although the diamond shape has one inclined interface, it has maximum about 50 percent interface failure. The circular shape has maximum 85 percent debonding (See Figs. 6.6 and 6.7). Both internal and boundary RVEs showed similar results as discussed above except for the diamond shape. This shape showed about 90 percent debonding along the interface for the internal RVE while about 50 percent for the boundary RVE. The reduced effective elastic modulus variation for both internal and boundary RVEs gave very close results for each shape of reinforcements individually. A slight exception to that was, the circular shape gave slightly different results between 15 and 50 degrees for internal and boundary RVEs.

The analysis of reduced effective elastic modulus variation using the internal RVE shows that circular and diamond shape reinforcements have close values of the effective elastic module at different debonding ratios. Although the square shape

reinforcement has minimum overall debonding, it shows the stiffest reduction in the effective elastic modulus (Figure. 6.8). This shows that, although the vertical interface section does not separate due to compression, it does not have major effect on the effective elastic modulus as much as inclined interface section. For the boundary RVE, the circular and octagonal shapes had similar reduction of effective moduli at a given debonding ratio as shown in Figure 6.9.

C.   FAILURE CRITERIA OF COMPOSITES FOR MULTIPLE REINFORCEMENT CASE

In the analysis of multiple reinforced composite materials, double circular shape reinforcements were studied for three different shear modulus ratios. In one of the two different cases the reinforcements had 20% volume fractions each, and in the second one, the reinforcements had 30% and 10% volume fractions. The same failure criterion, which was used for single reinforcement cases, was used for multiple reinforcement case also. The failure stresses for unit displacement boundary condition were plotted for each case and three different shear modulus ratios in Figs. 6.10 and 6.11. The values were normalized by the average failure stress value of the single circular reinforcement material for a better comparison. From the plots, it is observed that the stresses along the interface of the reinforcement of the larger size are 50% higher while the stresses along the interface of the reinforcement of the smaller size are 50% lower when compared to the stresses along the interface of the reinforcement with a 20% volume fraction. So, it is obvious that the failure will initiate along the interface of the reinforcement material that has higher volume fraction. Consequently, if the two cases are compared to each other for the same total reinforcement volume fraction, equal size reinforcements had lower failure stresses and higher effective elastic modulus than the different sized reinforcements.
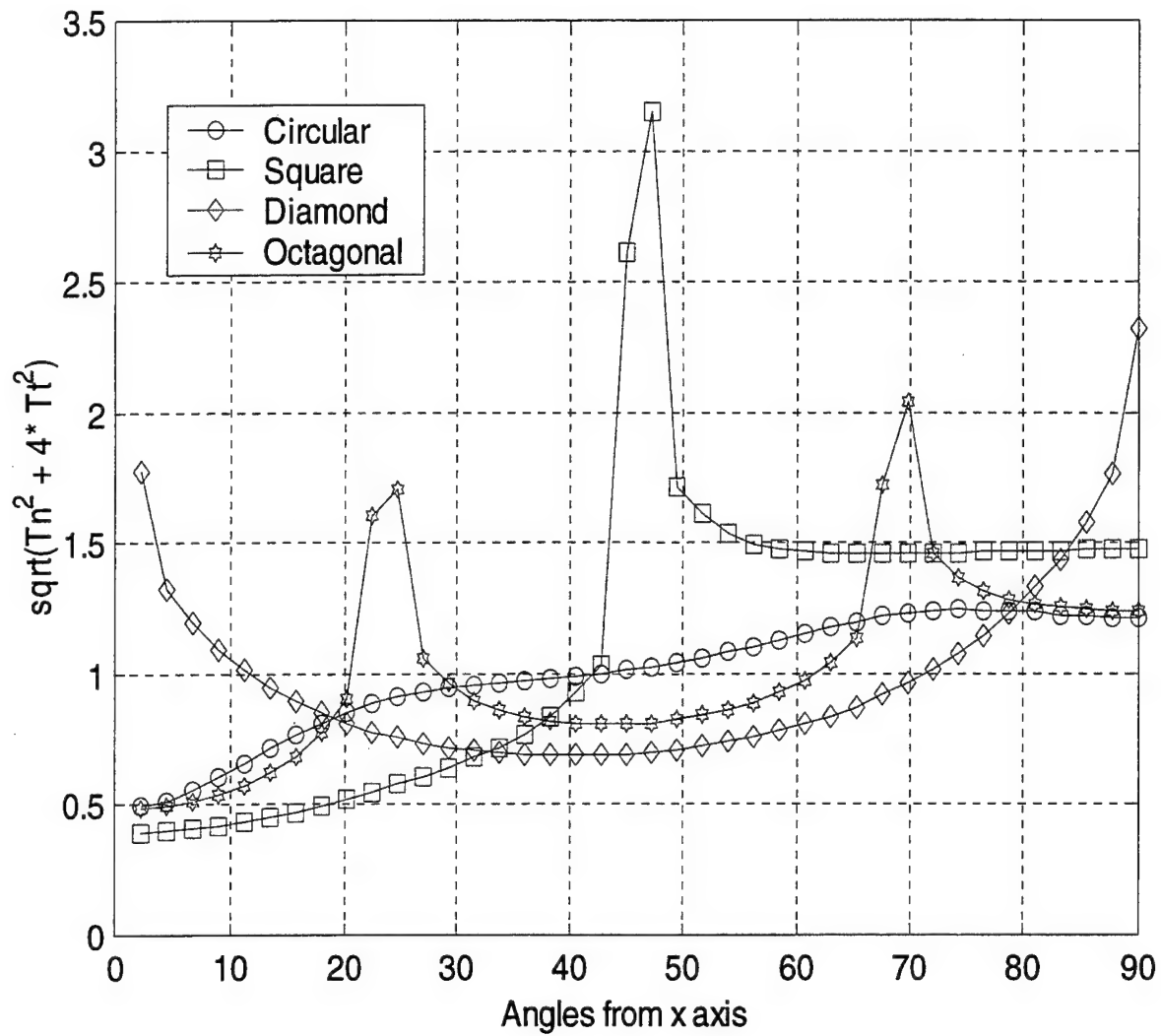
Figure 6.1: The Failure Stresses of Different Shapes of Reinforcement Elements Normalized by the Average Failure Stress of Circular Shape Reinforcement for Internal RVE.
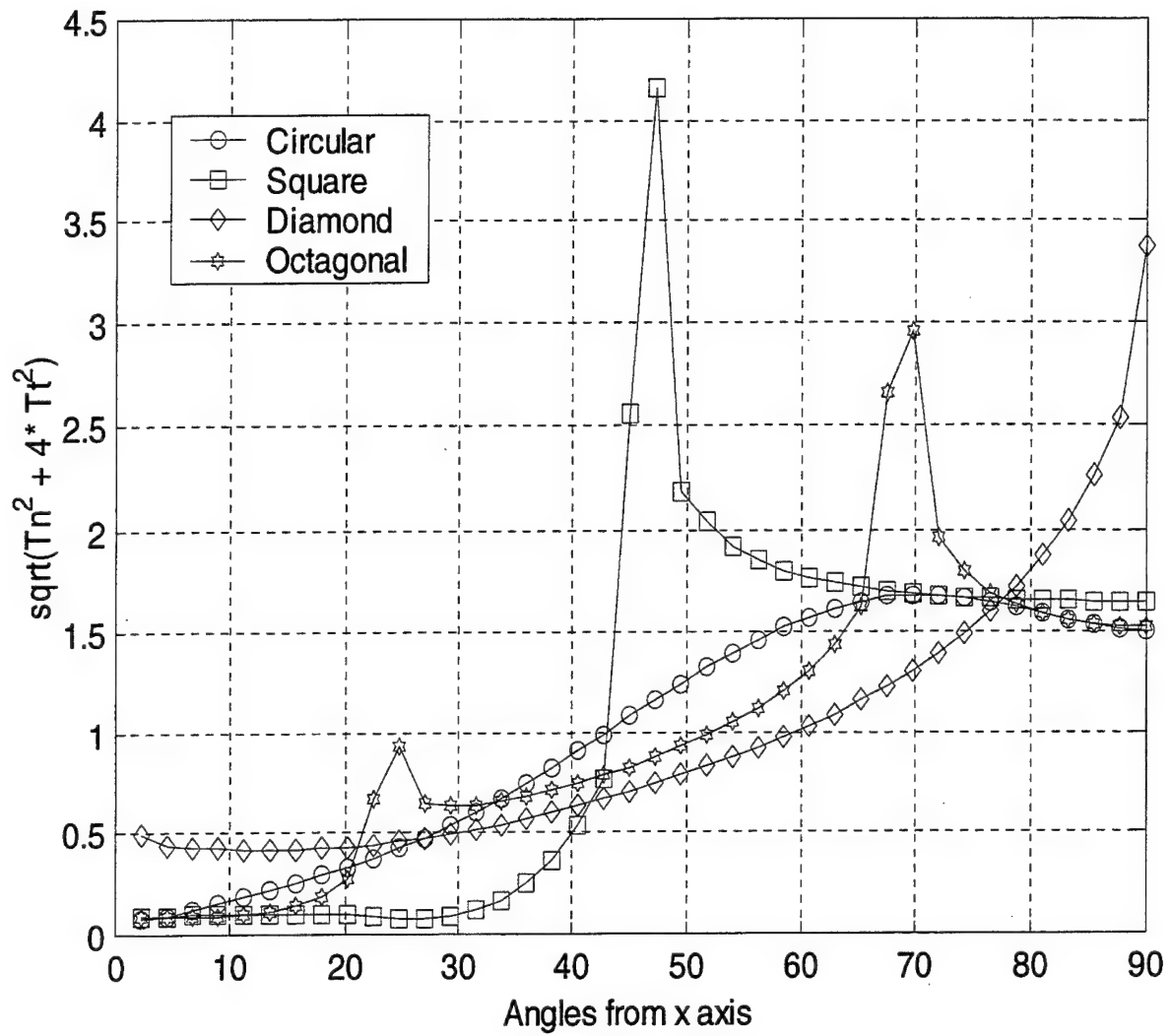
Figure 6.2: The Failure Stresses of Different Shapes of Reinforcement Elements Normalized by the Average Failure Stress of Circular Shape Reinforcement for Boundary RVE.
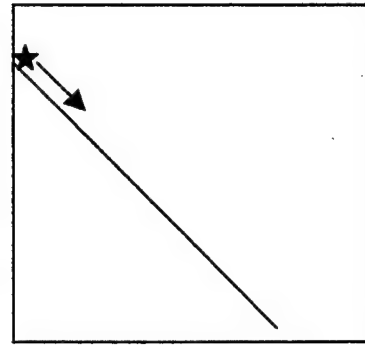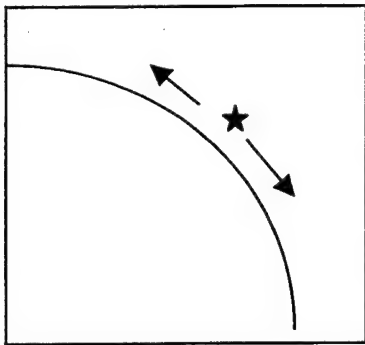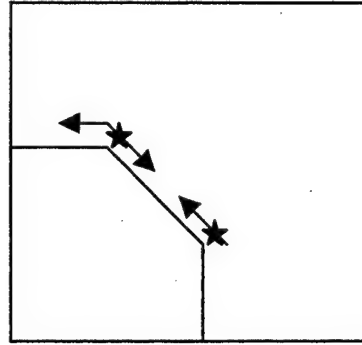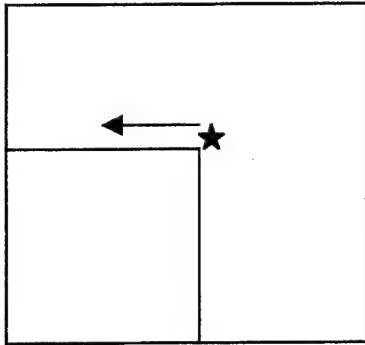
Figure 6.3: Debonding Initiation and Progress Cites for Different Shapes of Reinforcements, shown as Stars and Arrows.
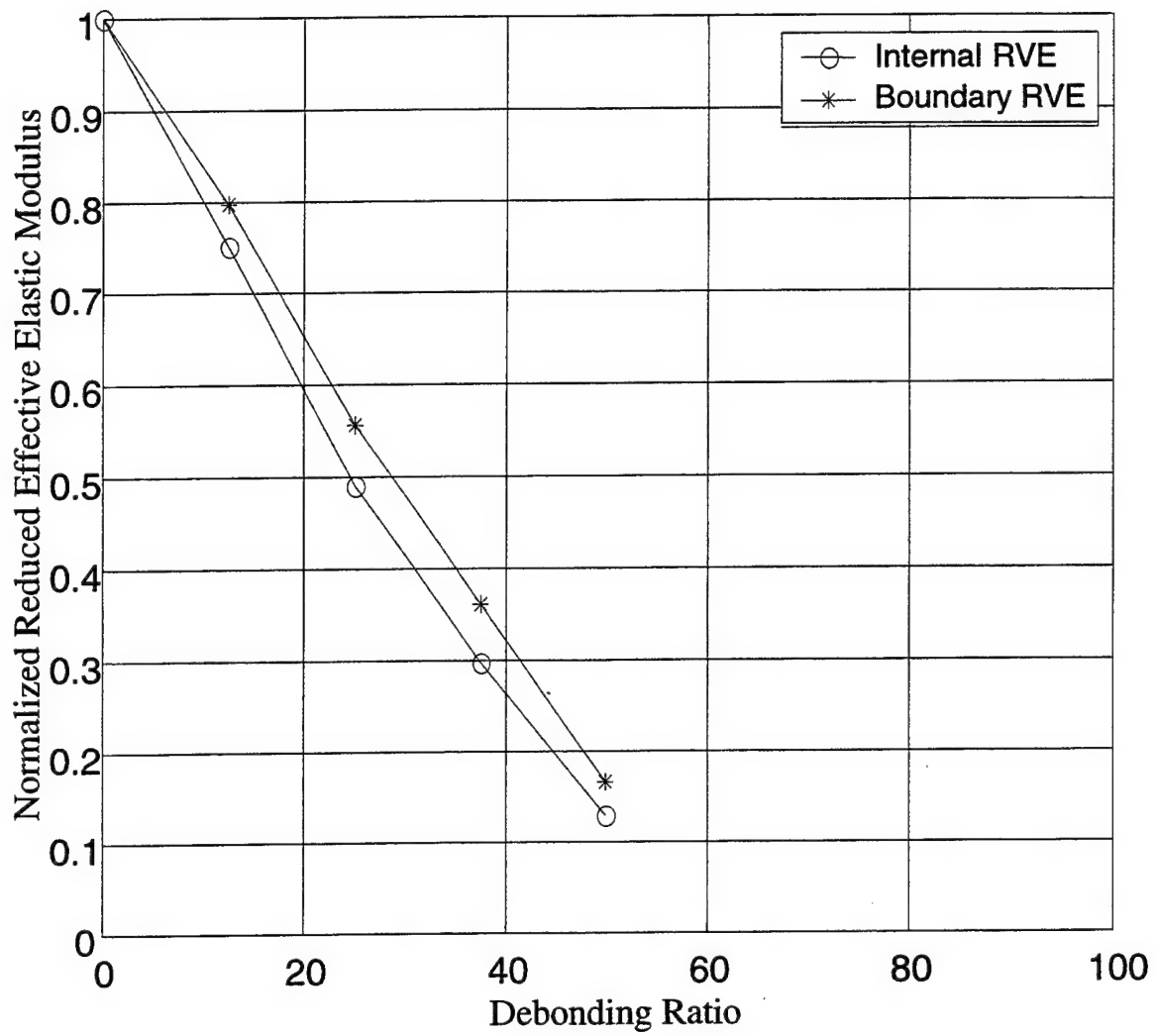
Figure 6.4: The Effective Elastic Modulus Variation for Square Shape Reinforcement Element at Different Debonding Ratios for Internal and Boundary RVEs.
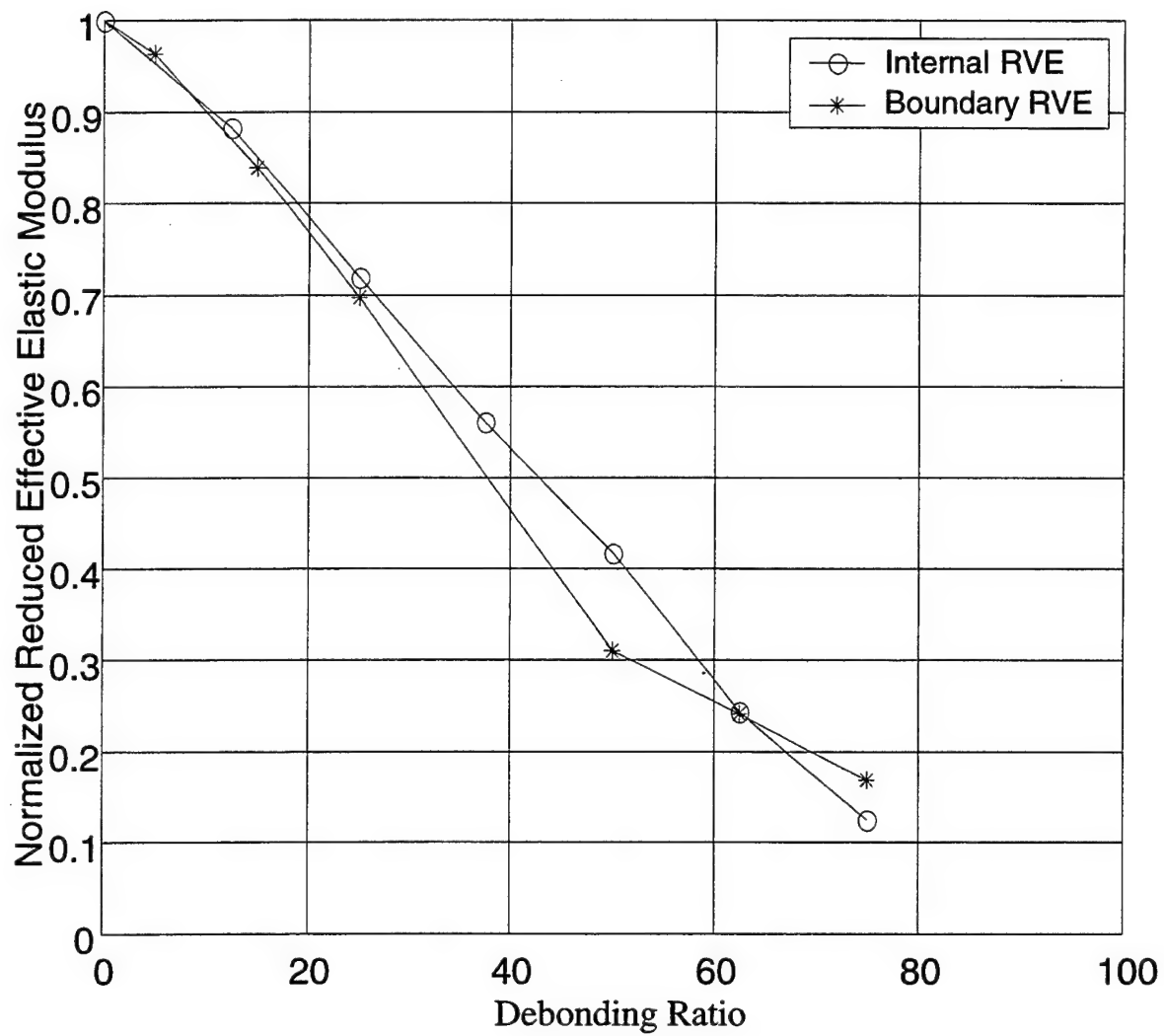
Figure 6.5: The Effective Elastic Modulus Variation for Octagonal Shape Reinforcement Element at Different Debonding Ratios for Internal and Boundary RVEs.
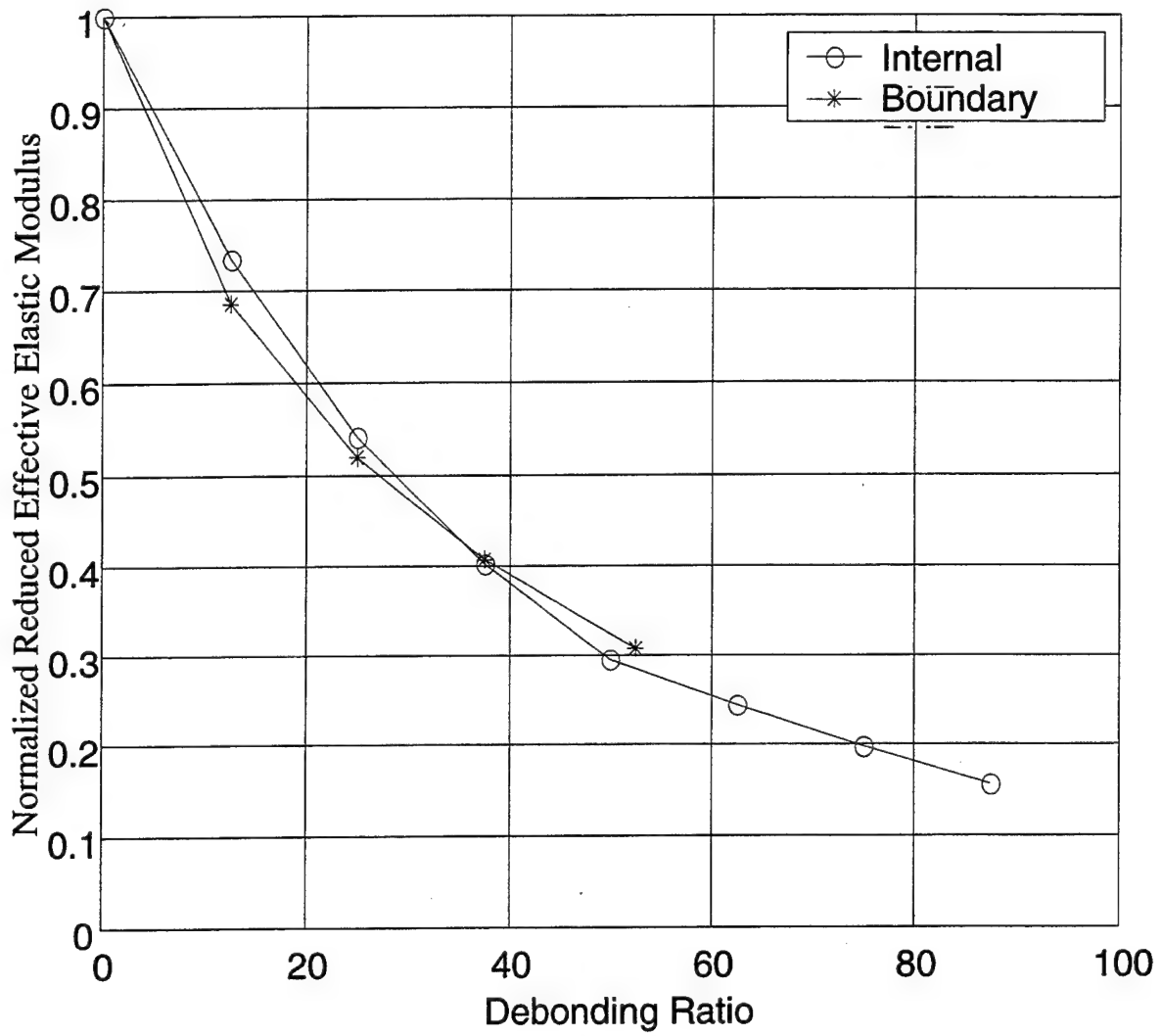
Figure 6.6: The Effective Elastic Modulus Variation for Diamond Shape Reinforcement Element at Different Debonding Ratios for Internal and Boundary RVEs.

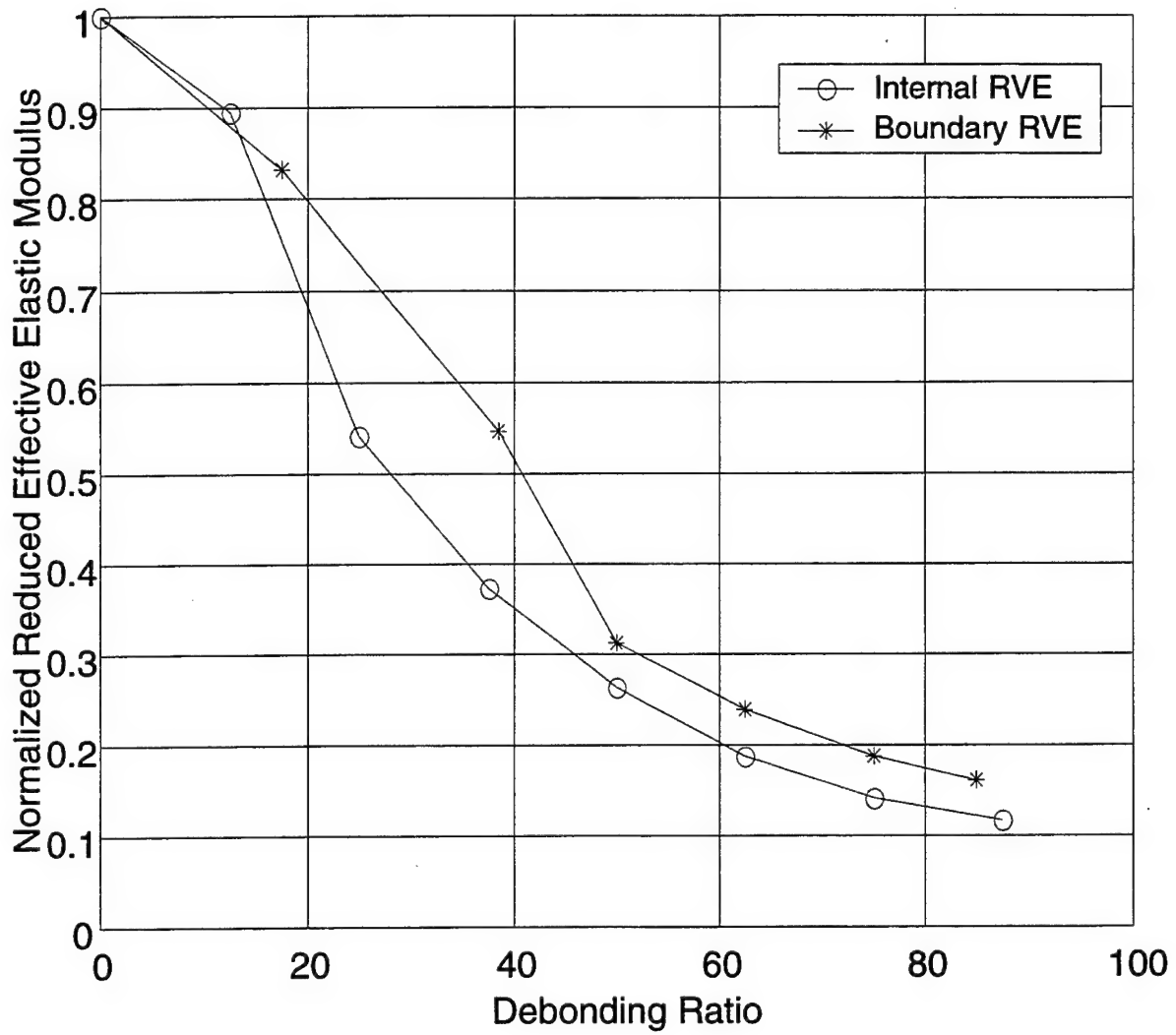Figure 6.7: The Effective Elastic Modulus Variation for Circular Shape Reinforcement Element at Different Debonding Ratios for Internal and Boundary RVEs.

Figure 6.8: The Effective Elastic Modulus Variation of Four Reinforcement Shapes During the Progress of Failure for Internal RVE.
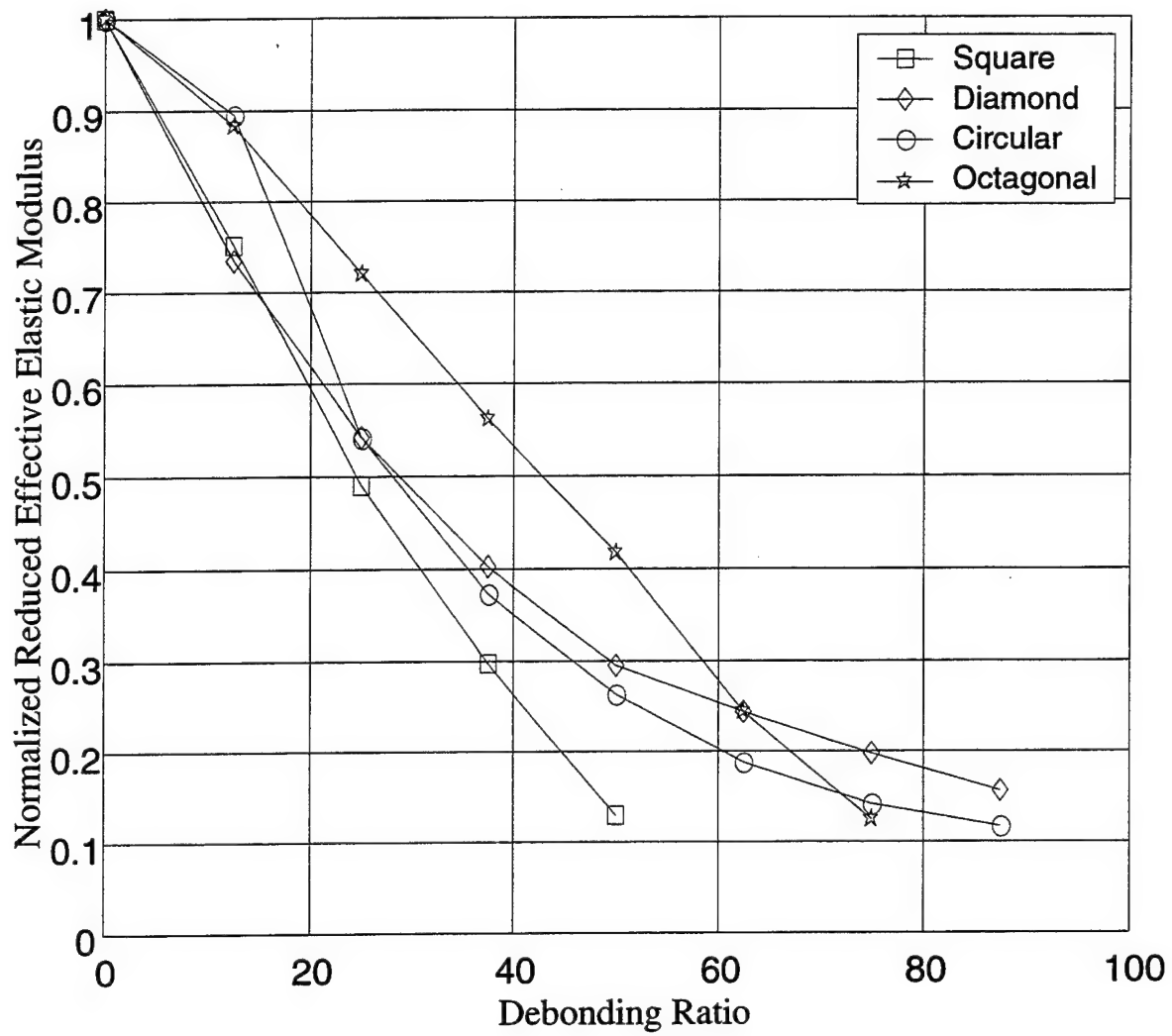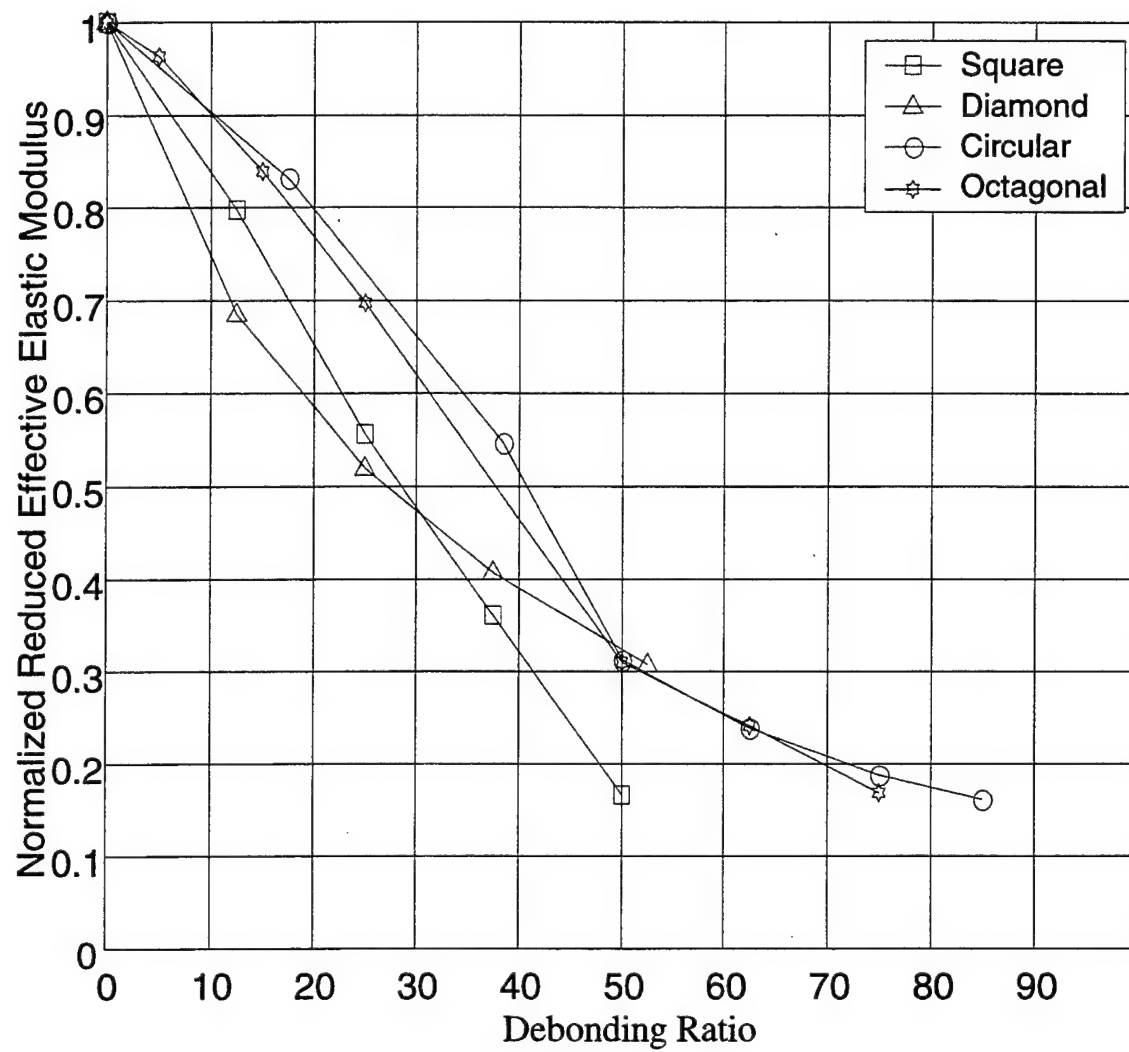
Figure 6.9: The Effective Elastic Modulus Variation of Four Reinforcement Shapes During the Progress of Failure for Boundary RVE.

Figure 6.10: The Failure Stresses Along the Interfaces of Equal Size Reinforcement Elements (20% each), Normalized by the Average Failure Stress of Single Circular Reinforcement for Three Different Shear Modulus Ratios.

Figure 6.11: The Failure Stresses Along the Interfaces of Different Size Reinforcement Elements (30% and 10%), Normalized by the Average Failure Stress of Circular Shape Reinforcement for Three Different Shear Modulus Ratios.

THIS PAGE INTENTIONALLY LEFT BLANK

VII. CONCLUSIONS AND RECOMMENDATIONS

Some of important results from the present analysis are summarized below:
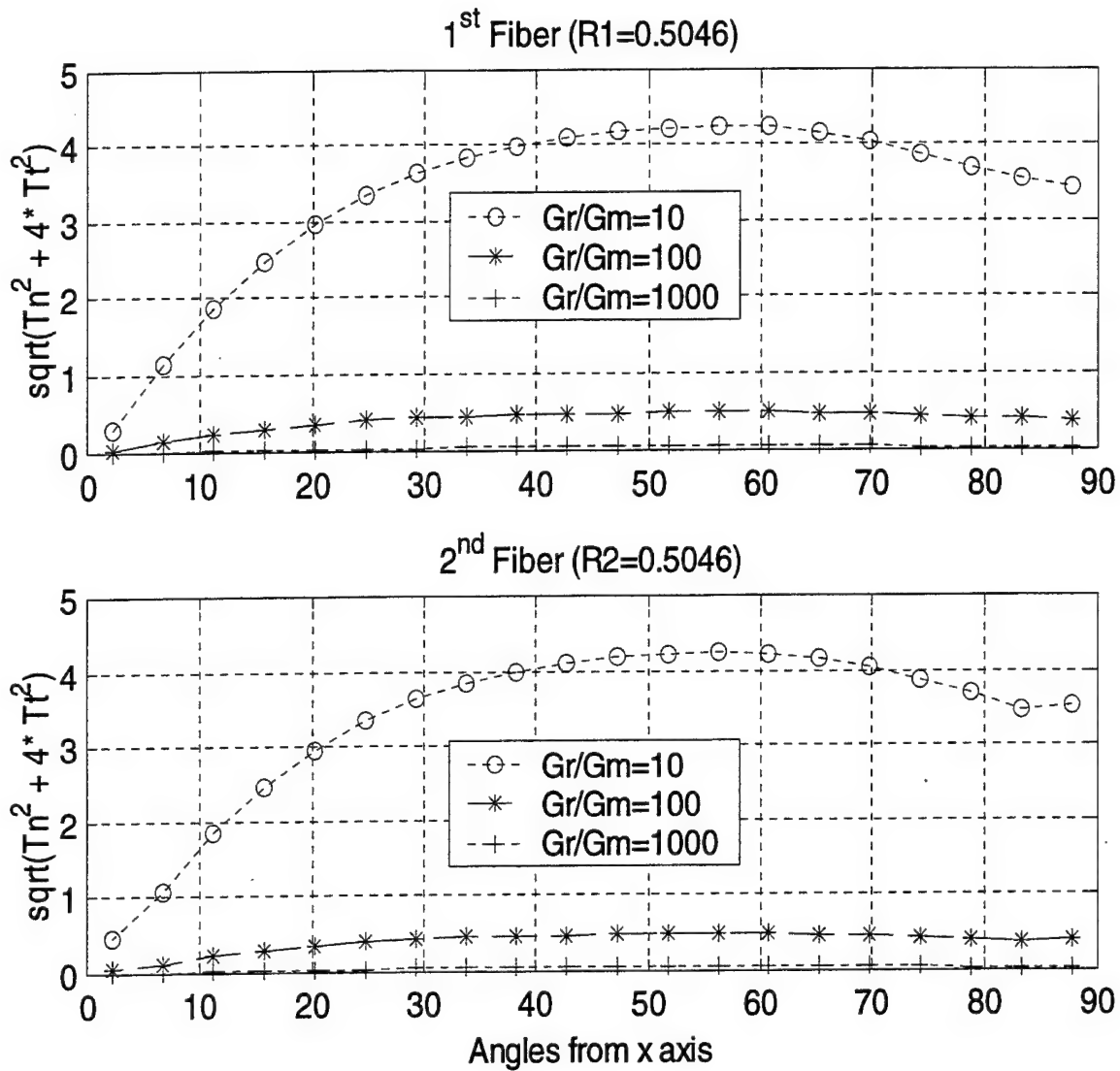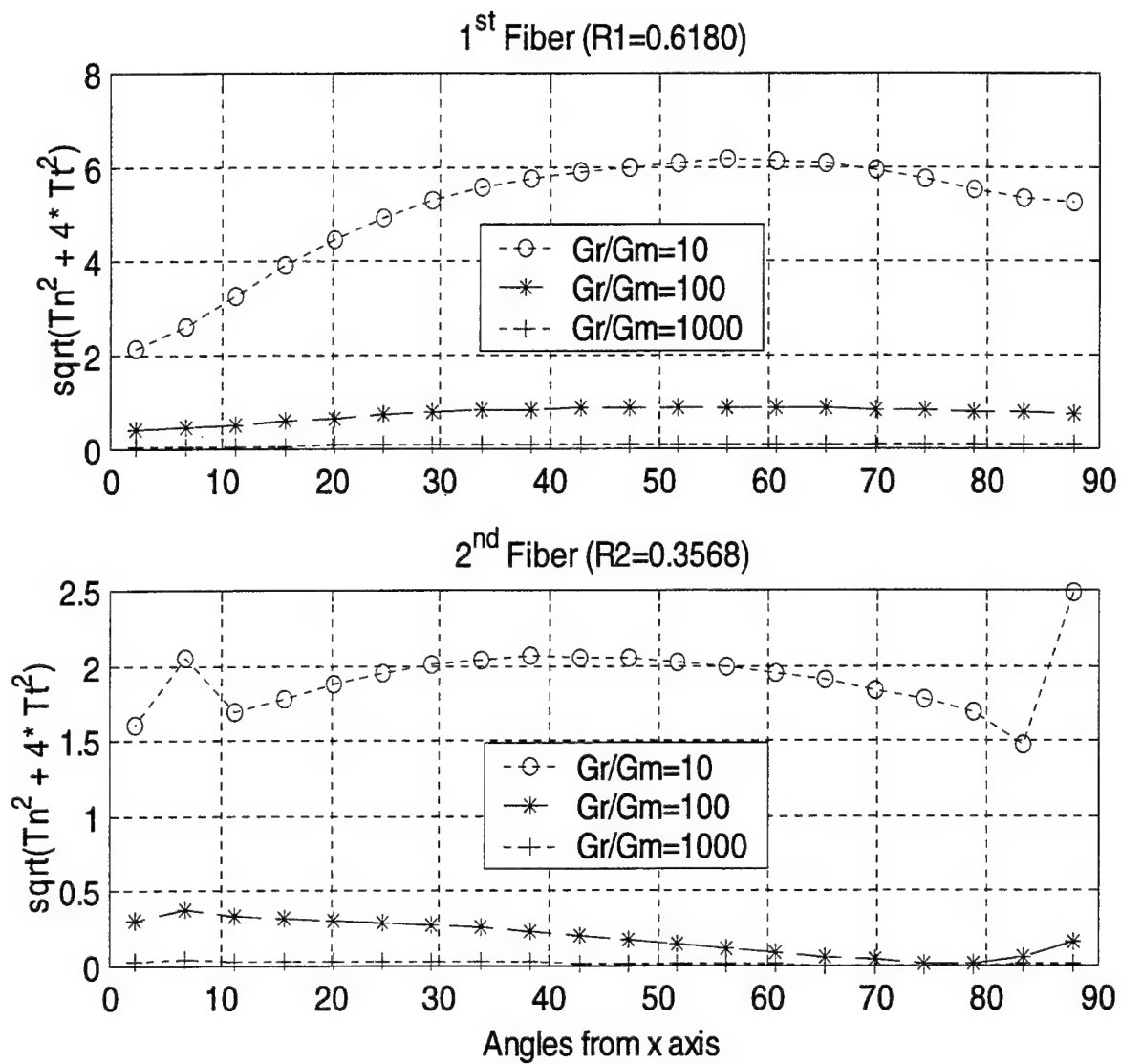
1.   The stress values along the interfaces of internal RVEs are higher than those of boundary RVEs. Therefore, interfacial debonding may occur at inside of the composite material rather than the outside boundary. Among different shapes considered here, the square has the highest interface failure stresses even if the effect of stress concentration at the corner is not considered.

2.   The interface normal stress distribution was approximately constant for each linear segment of the interfaces of square, octagonal and diamond shapes if the stress concentration is discarded. As the number of linear segments of a polygonal shape of reinforcement increases, the normal stress distribution should approach to that for the circular shape of reinforcement.

3.   It was observed that Poisson's ratio of the matrix material played a very important role in the effective elastic modulus of a composite. A small change in Poisson's ratio of the matrix material causes a big difference in the elastic modulus of a composite material. The change in the shear modulus ratio of the reinforcement to the matrix materials (G_r/G_m) does not affect the effective elastic modulus of the composite material very much after a certain threshold value of the ratio if the reinforcement volume fraction is relatively low.

4.   The normalized normal stress distribution along the interface has a small variation for different reinforcement volume fraction when the ratio (G_r/G_m) is 10. The variation is smaller for the internal RVE than for the boundary RVE. However, there is more dramatic difference in the shear stress distribution among different reinforcement volume

fractions. When the ratio (G_r/G_m) is 100 and beyond, the normalized normal and shear stresses remain almost the same regardless of different ratios of (G_r/G_m) for each reinforcement volume fraction.

5.   Although the square shape reinforcement material gave the highest effective elastic modulus, it was the most susceptible shape to go under debonding initiation and progress, and gave the stiffest reduction in the effective elastic modulus during the progress of failure. The circular shape was the least for debonding initiation.

6.   For the same fiber volume fraction, the single reinforcement case gave a higher effective elastic modulus than the double reinforcement case, and within double reinforcement cases, the equal size reinforcement gave a higher effective elastic modulus than different size reinforcements. In terms of the interface stresses, the single reinforcement has the largest stress, and the two equal sizes of double reinforcements have the smallest stress. That is, the single reinforcement model is stiffer but more susceptible for interface damage.

This study can be extended to model more multiple reinforcements and orientations. The shapes used in this study can be re-analyzed by rounding their corners. Interface failure criteria need to be further examined because they are important to determine potential failure at the interface. Some experimental work is recommended to evaluate the analytical study conducted here.

LIST OF REFERENCES

1. Achenbach, J., D., ZHU, H., Effect of Interfacial Zone on Mechanical Behavior and Failure of Fiber-Reinforced Composites, Journal of Mechanics and Physics of Solids, Vol. 37, No 3, pp 381-383, 1989.

2. Shen, Y., L., Finot, A., Needleman, A., Suresh, S., Effective Elastic Response of Two-Phase Composites, Acta Metall. Mater., Vol 42, No 1, pp 77-97, 1994.

3. Pan, L., Adams, O., D., Rizzo, J., F., Boundary Element Analysis for Composite Materials and a Library of Green's Functions, Computers & Structures, Vol. 66, No. 5, pp. 685-693, 1998.

4. Banerjee, P., K., Henry, D., P., Hopkins, D., A., Goldberg, R., K., Further developments of BEM for Micro and Macro mechanical Analysis of Composites, NASA Grant No. NAG3-1483, April 1993-March 1997.

5. Brebbia, C. A., Dominguez, J., Boundary Elements An Introductory Course, McGraw-Hill Book Company, Great Britain, 1989.

6. Muskhelishvili, N., I., Some Basic Problems of the Mathematical Theory of Elasticity, P., Noordhooff Ltd., Groningen, Holland, 1953.

7. Tsai, S., W., Hahn, H., T., Introduction to Composite Materials, Technomic Publication, USA, 1980.

8. Kwon, Y., W., Kim, C., Micro mechanical Model for Thermal Analysis of Particulate and Fibrous Composites, Journal of Thermal Stresses, Vol. 21, pp 21-39, 1998.

9. Gibson, R., F., Principles of Composite Material Mechanics, McGraw Hill inc., USA, 1994.

10. Aboudi, J., Micro mechanical Analysis of Composites by the Method of Cells, Appl. Mech. Rev. vol. 42, no 7, pp 193-221, 1989.

THIS PAGE INTENTIONALLY LEFT BLANK

INITIAL DISTRIBUTION LIST

1. Defense Technical Information Center 2
    8725 John J. Kingman Rd., STE 0944
    Ft. Belvoir, Virginia 22060-6218

2. Dudley Knox Library 2
    Naval Postgraduate School
    411 Dyer Rd.
    Monterey, CA 93943-5101

3. Proffesor Young W. Kwon , Code ME/Kw 2
    Department of Mechanical Engineering
    Naval Postgraduate School
    Monterey, CA93943

4. Department Chairman, Code ME 1
    Department of Mechanical Engineering
    Naval Postgraduate School
    Monterey, CA93943

5. Engineering and Technology Curriculum Code 34 1
    700 Dyer Rd., Building 245
    Monterey, CA 93943-5100

6. Ltjg Hakan Eren 2
    Izmir Tersanesi Komutanligi
    Plan Kesif Dizayn Sb. Md.
    Tahrik Sistem Sb.
    Izmir, Turkey

7. Ltjg. Ahmet Altekin 1
    Engineering and Technology Curriculum Code 34
    700 Dyer Rd., Building 245
    Monterey, CA 93943-5100